

# The dust content of damped Lyman- $\alpha$ systems in the Sloan Digital Sky Survey

Michael T. Murphy,<sup>1</sup><sup>★</sup> Martin L. Bernet<sup>1,2</sup>

<sup>1</sup>*Centre for Astrophysics and Supercomputing, Swinburne University of Technology, Hawthorn, Victoria 3122, Australia*

<sup>2</sup>*Physics Department, ETH Zurich, Wolfgang-Pauli-Strasse 27, CH-8093 Zurich, Switzerland*

Accepted 2015 October 16. Received 2015 October 15; in original form 2015 September 04

## ABSTRACT

The dust-content of damped Lyman- $\alpha$  systems (DLAs) is an important observable for understanding their origin and the neutral gas reservoirs of galaxies. While the average colour-excess of DLAs,  $E(B-V)$ , is known to be  $\lesssim 15$  milli-magnitudes (mmag), both detections and non-detections with  $\sim 2$  mmag precision have been reported. Here we find  $3.2\text{-}\sigma$  statistical evidence for DLA dust-reddening of 774 Sloan Digital Sky Survey (SDSS) quasars by comparing their fitted spectral slopes to those of  $\sim 7000$  control quasars. The corresponding  $E(B-V)$  is  $3.0 \pm 1.0$  mmag, assuming a Small Magellanic Cloud (SMC) dust extinction law, and it correlates strongly ( $3.5\text{-}\sigma$ ) with the metal content, characterised by the Si II  $\lambda 1526$  absorption-line equivalent width, providing additional confidence that the detection is due to dust in the DLAs. Evolution of  $E(B-V)$  over the redshift range  $2.1 < z < 4.0$  is limited to  $< 2.5$  mmag per unit redshift ( $1\text{-}\sigma$ ), consistent with the known, mild DLA metallicity evolution. There is also no apparent relationship with neutral hydrogen column density,  $N_{\text{H I}}$ , though the data are consistent with a mean  $E(B-V)/N_{\text{H I}} = (3.5 \pm 1.0) \times 10^{-24}$  mag cm<sup>2</sup>, approximately the ratio expected from the SMC scaled to the lower metallicities typical of DLAs. We implement the SDSS selection algorithm in a portable code to assess the potential for systematic, redshift-dependent biases stemming from its magnitude and colour-selection criteria. The effect on the mean  $E(B-V)$  is negligible ( $< 5$  per cent) over the entire redshift range of interest. Given the broad potential usefulness of this implementation, we make it publicly available.

**Key words:** dust, extinction – galaxies: high redshift – intergalactic medium – galaxies: ISM – quasars: absorption lines

## 1 INTRODUCTION

Currently, the only direct way to probe the neutral gas surrounding early galaxies is to study its absorption against background objects. Damped Ly- $\alpha$  systems (DLAs) – defined as having a neutral hydrogen column densities of  $N_{\text{H I}} = 2 \times 10^{20}$  cm<sup>-2</sup> in absorption (Wolfe et al. 1986) – provide rich information about this gas, particularly when observed along the sight-lines to quasars, i.e. relatively bright, very compact objects. At such column densities, the gas in DLAs is self-shielded against the ultraviolet background radiation from galaxies and quasars, so it is predominantly neutral (e.g. Viegas 1995), enabling very precise metallic element abundances to be measured. However, some metals (e.g. C, Mg, Fe, Cr) will be preferentially incorporated into dust grains (Jenkins 1987; Pettini et al. 1997), so a complete and accurate understanding of the nucleosynthetic history of

DLA gas requires some knowledge of its dust content. This is also an important factor in identifying possible  $\alpha$ -element enhancements in DLAs (e.g. Vladilo 2002; Ledoux et al. 2002). Further, dust grains are the formation sites for most molecular hydrogen in cool DLA gas (Jenkins & Peimbert 1997; Ledoux et al. 2003) and provide surfaces for photoelectric heating of DLAs (Wolfe et al. 2003a,b). Understanding the dust content of DLAs is therefore important for determining their astrophysical origins and significance.

DLAs are cosmologically important because they contain most of the neutral gas at all redshifts up to at least  $z = 5$  (e.g. Wolfe 1986; Lanzetta et al. 1995; Prochaska et al. 2005; Prochaska & Wolfe 2009; Noterdaeme et al. 2009b; Crighton et al. 2015). However, if dust in DLAs obscures a significant proportion of the background quasars from flux-limited and/or colour-selected quasar surveys (Ostriker & Heisler 1984), the comoving mass density of DLA gas,  $\Omega_{\text{g}}^{\text{DLA}}$ , will be underestimated (e.g. Fall & Pei 1993). This may be a particularly acute concern if, as one may naively expect,

<sup>★</sup> E-mail: mmurphy@swin.edu.au (MTM)

higher- $N_{\text{H I}}$  DLAs contain more dust, because DLAs with  $N_{\text{H I}} \sim 10^{21} \text{ cm}^{-2}$  have the largest contribution to  $\Omega_{\text{g}}^{\text{DLA}}$  despite their relative paucity (e.g. see figures 10 and 14 of Prochaska et al. 2005 and Noterdaeme et al. 2009b, respectively). Surveys of DLAs in radio-selected quasar samples avoid dust bias, though obtaining large enough samples is much more difficult. For example, the combined samples of Ellison et al. (2005) and Jorgenson et al. (2006) contain 26 DLAs identified towards 119 quasars and yield a  $\Omega_{\text{g}}^{\text{DLA}}$  which is a factor of  $\sim 1.3$  higher than optically-selected surveys, but with a 33 per cent uncertainty. Therefore, attempts to determine  $\Omega_{\text{g}}^{\text{DLA}}$  with  $\lesssim 20$  per cent accuracy must incorporate other, possibly tighter constraints on DLA dust content.

The most direct indicators of dust in DLAs would be the carbonaceous 2175 Å ‘dust bump’ absorption feature and the silicate dust features at 10 and 18  $\mu\text{m}$  (e.g. Draine 2003). The dust bump is ubiquitous in Milky Way studies but less prominent in sight-lines through the Large Magellanic Cloud (LMC) and seemingly absent in the Small Magellanic Cloud (SMC). Given the broad undulations and small variations in quasar continua, clear dust bump detections are difficult and rare. Indeed, just three detections in bona fide DLAs have been reported (Junkkarinen et al. 2004; Noterdaeme et al. 2009a; Ma et al. 2015), though several have been reported in strong Mg II absorbers (e.g. Wang et al. 2004; Zhou et al. 2010; Jiang et al. 2010; Wang et al. 2012). The silicate features are also rare: the 10  $\mu\text{m}$  feature has been detected in two bona fide DLAs (Kulkarni et al. 2007, 2011) and 5 other strong quasar absorbers (Kulkarni et al. 2011; Aller et al. 2012, 2014). Using these features to determine the average DLA dust content appears unlikely, if not impossible, though they clearly allow the chemical and physical characteristics of the dust in some DLAs to be studied.

The average DLA dust content may be better determined by measuring the reddening it should impart to the spectra of the background quasars. The significant variation in quasar colours means that this is an inherently statistical approach, with large samples of quasars with foreground DLAs (‘DLA quasars’) and, importantly, larger samples without DLAs (‘non-DLA quasars’) to act as ‘controls’, required to detect small amounts of dust. Early attempts (Fall & Pei 1989; Fall et al. 1989) culminated in a  $>4\text{-}\sigma$  detection of average DLA reddening of  $\Delta\beta = 0.38 \pm 0.13$  (Pei et al. 1991) with 26 DLA quasars and 40 non-DLA quasars, where  $\beta$  represents the spectral index when the quasar continuum flux density is fitted as

$$f_{\lambda} \propto \lambda^{\beta}. \quad (1)$$

This implied that 10–70 per cent of bright quasars at redshift  $z = 3$  were being missed in optical surveys (Fall & Pei 1993). The Sloan Digital Sky Survey (SDSS) increased the available DLA and non-DLA quasar samples significantly and ensured a more uniform quasar selection. Using 70 DLA quasars and  $\sim 1400$  non-DLA quasars, Murphy & Liske (2004) found no evidence for DLA dust reddening at  $2.1 < z < 3.9$ , with  $\Delta\beta$  constrained to be  $< 0.19$  at  $3\text{-}\sigma$  confidence, inconsistent with previous results. Assuming an SMC dust reddening law, the rest-frame colour excess of DLA dust reddening was limited to  $E(B-V)_{\text{SMC}} < 20$  milli-magnitudes (mmag) at  $3\text{-}\sigma$  confidence. This stringent limit indicates a very low average DLA dust content and illustrates the large, careful analysis required to detect dust via this statistical approach.

More recent SDSS-based analyses have provided a mix of apparent detections and other limits on DLA dust reddening at similar redshifts ( $2.2 \lesssim z \lesssim 3.5$ ). Using the photometric colours of 248 DLA quasars from the SDSS Data Release (DR) 5, Vladilo et al. (2008) found a  $\approx 3.5\text{-}\sigma$  indication of reddening with rest-frame  $E(B-V)_{\text{SMC}} \approx 6$  mmag. Frank & Péroux (2010) compared composite spectra, made from stacking DR7 spectra in the rest-frame of 676 DLAs, with composites from non-DLA quasars ‘matched’ in redshift and magnitude. This indicated no DLA reddening,  $E(B-V)_{\text{SMC}} = -1.7 \pm 2.2$  mmag,  $\approx 2.9\sigma$  lower than Vladilo et al. (2008)’s result. Khare et al. (2012) performed a similar analysis using 1084  $\log(N_{\text{H I}}/\text{cm}^{-2}) \geq 20.0$  absorbers [i.e. including ‘sub-DLAs’, or ‘super Lyman-limit systems’, with  $20.0 \leq \log(N_{\text{H I}}/\text{cm}^{-2}) < 20.3$ ], finding no evidence for reddening from the absorbers, consistent with Frank & Péroux. Most recently, Fukugita & Ménard (2015) used the photometric colours of 1211 sub-DLA and DLA quasars from DR9 in the restricted absorption redshift range  $2.1 < z_{\text{abs}} < 2.3$ , finding a relatively large  $E(B-V)_{\text{SMC}} \approx 10$  mmag with  $\sim 4\text{-}\sigma$  significance. These recent results are discussed further in Section 6.

Given the variety of recent results, it is important to further consider the average dust content of DLAs. Here we use DR7 spectra to measure the spectral index,  $\beta$  in equation (1), and hence  $E(B-V)$  for an assumed dust extinction law, in 774 SDSS DLA quasars. We also constrain how the dust content depends on redshift, gas column density and metal-line strength with the aim of finding clues to the origin and physical/chemical nature of the dust and the DLAs themselves. However, as with previous SDSS-based studies, we must recall that the SDSS quasars targeted for spectroscopy were selected based on their colours. In principle, this could lead to a bias towards or against dusty DLAs (i.e. redder spectra) in the SDSS quasar sample. Given the complicated, redshift-dependent nature of the colour-selection algorithm (Richards et al. 2002), this bias should also be redshift-dependent. Here we consider in detail the effect of colour selection bias on the measured colour excess from DLA dust for the first time. We demonstrate the effect to be negligible at all redshifts we consider ( $2.1 < z_{\text{abs}} < 4.0$ ).

This paper is organised as follows. Section 2 describes the quasar and DLA samples used in this work and how control samples were established for all DLA quasars. Section 3 explains how the spectral index and colour excess were measured for each DLA. Section 4 details the main results while discussion and comparison with other recent results is deferred to Section 6. We test the effects of colour-selection bias in Section 5 and Appendix A describes our emulation of the SDSS quasar colour selection algorithm of Richards et al. (2002) and basic tests to ensure its reliability for this work. Given the broad potential usefulness of this code, we have provided it in Bernet & Murphy (2015). Our main conclusions are summarized in Section 7.

## 2 QUASAR AND DLA SAMPLE DEFINITIONS

### 2.1 Quasar catalogues, spectra and exclusions

The results presented in this paper are derived from the SDSS DR7 versions of the spectra identified as quasars in the

catalogue of Schneider et al. (2010). This catalogue contains 105783 quasars with improved (where necessary) emission redshift measurements compared with those automatically determined by the original SDSS data processing system. We exclude the 6214 broad absorption line (BAL) quasars identified in this catalogue by Shen et al. (2011) because the BAL features may have interfered with the DLA identification procedure (see Section 2.2) and because BAL quasars are often heavily reddened compared to the normal distribution of quasar colours (e.g. Reichard et al. 2003). We also exclude quasars with emission redshifts outside the range  $2.20 \leq z_{\text{em}} \leq 4.42$ . The lower redshift cut ensures a non-zero search path for DLAs redwards of the blue limit of the SDSS spectra (i.e.  $\approx 3800 \text{ \AA}$ ) while the higher redshift cut ensures that the reddest band we use to determine the quasar spectral index (quasar rest-frame wavelengths 1684–1700  $\text{\AA}$ ; see Section 3) remains entirely bluewards of the red limit of the SDSS spectra (i.e.  $\sim 9200 \text{ \AA}$ ). These redshift restrictions leave 14672 quasars (note the further restrictions on the quasar sample below in Section 2.2).

We also cross-checked our main results using both the DR5 and DR7 spectra of the quasars identified in the DR5 quasar catalogue of Schneider et al. (2007), and find consistent results. A new reduction and spectrophotometric calibration was introduced in DR6, yielding a 30 mmag root-mean-square (RMS) difference between the  $r-i$  colours from the point-spread-function (PSF) photometry and those synthesized from the calibrated spectra of stars<sup>1</sup>. The spectrophotometry of DR9 spectra is expected to be biased because smaller fibres were used (2 vs. 3" diameter, respectively) and, without atmospheric dispersion compensation available, they were offset to collect blue light at the expense of red light to probe the Ly- $\alpha$  forest (Pâris et al. 2012).

## 2.2 DLA samples

The baseline results in this paper were derived using DLAs from the catalogue of Noterdaeme et al. (2009b). They searched DR7 spectra of objects that the automatic SDSS data processing labelled as quasars with  $z_{\text{em}} > 2.17$ . The search was restricted to 8339 spectra with median continuum-to-noise ratios (CNRs) exceeding 4 per pixel ( $\text{pix}^{-1}$ ) redwards of the wavelength where the signal-to-noise ratio (SNR) first exceeds  $4 \text{ pix}^{-1}$ . Noterdaeme et al. (2009b) applied an automated algorithm to detect DLAs and determine their  $z_{\text{abs}}$ ,  $N_{\text{H I}}$  and rest equivalent widths of selected metal lines, e.g.  $W_r(\text{C II } \lambda 1334)$  and more often  $W_r(\text{Si II } \lambda 1526)$ .

From the 14672 DR7 quasars selected in Section 2.1 we removed the 6743 quasars that were not among those searched for ‘strong absorbers’ by Noterdaeme et al. (2009b), leaving 7929 quasars. These ‘strong absorbers’ include DLAs and sub-DLAs systems with  $\log(N_{\text{H I}}/\text{cm}^{-2}) \geq 20.0 \text{ cm}^{-2}$ . Our main results and much of our discussion below focus on the DLAs only. However, as a cross-check on possible systematic effects and to boost sample sizes when searching for trends within our results, we also perform the same analyses with the sub-DLAs included.

<sup>1</sup> See description at <http://www.sdss2.org/dr7/algorithms/spectrophotometry.html>.

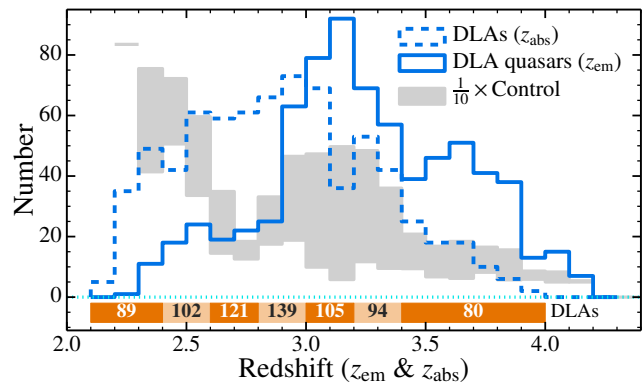


**Figure 1.** Emission redshift ( $z_{\text{em}}$ ) distributions of DLA quasars (solid line) and their corresponding control quasars (shaded regions), and the absorption redshift ( $z_{\text{abs}}$ ) distribution of the DLAs themselves. There is a single DLA per DLA quasar. For each  $\Delta z = 0.1$  bin, the shaded region indicates the range in sizes of the control samples for the DLA quasars in that bin. Note that these shaded regions are normalized by a factor of 10 for clarity; for example, the minimum and maximum number of control quasars corresponding to any of the DLA quasars with  $3.0 \leq z_{\text{em}} < 3.1$  is 99 and 473, respectively. The shaded bar below the histograms, labelled with the number of DLAs in each bin, shows the absorption redshift bins used in subsequent figures.

The final restriction on the quasar and absorber samples is to remove quasar spectra in which Noterdaeme et al. (2009b) identified more than one ‘strong absorber’. This last selection criterion defines our baseline samples as follows:

- **DLA & non-DLA samples:** 7879 quasars; 774 are DLA quasars (i.e. with a single, bona fide DLA); 7105 are non-DLA quasars.
- **Absorber & non-absorber samples:** 7802 quasars; 1069 are absorber quasars [i.e. with a single  $\log(N_{\text{H I}}/\text{cm}^{-2}) \geq 20.0 \text{ cm}^{-2}$  system]; 6733 are non-absorber quasars.

Note that this last criterion means that the DLA+non-DLA sample is larger than the absorber+non-absorber sample. This is because sub-DLAs are more common than DLAs, and because sub-DLAs are allowed in the DLA and non-DLA quasar spectra but only a single DLA or sub-DLA is allowed in the absorber quasars. That DLA quasars are allowed to be ‘contaminated’ by sub-DLAs is offset by the contamination of non-DLA quasars in the same way and in approximately equal proportion, thereby leaving a negligible residual effect on the differential reddening measurement we make in Section 3.

Tables 1–4 provide the relevant information for each of these samples, including the basic (sub-)DLA parameters used in the reddening analysis below. Figure 1 shows the redshift distributions of the DLA quasars and the DLAs themselves. Note the relative paucity of DLA quasars with  $z_{\text{em}} < 2.9$ : quasar colours cross the stellar locus between  $z_{\text{em}} \sim 2.5$ –3.0, so the SDSS colour-selection algorithm had to be specially modified there even to select some quasars. This is one example of the strongly varying, complicated quasar colour selection function in the SDSS. By comparison, Fig. 1 shows that the DLA redshift distribution is relatively smooth.

**Table 1.** The DLA quasar sample (774 quasars). The quasars are listed by their SDSS name (formed from right ascension and declination), emission redshift ( $z_{\text{em}}$ ), the redshift search path for DLAs defined by  $z_{\text{min}}$  and  $z_{\text{max}}$  [see equation (3)], the measured spectral index,  $\beta$ , and its  $1\text{-}\sigma$  uncertainty ( $\sigma_\beta$ ), and the spectral index measured with an unweighted power-law fit,  $\beta_{\text{nw}}$ . The DLA properties required in our analysis are the absorption redshift ( $z_{\text{abs}}$ ), logarithmic column density,  $N_{\text{H I}} \equiv \log(N_{\text{H I}}/\text{cm}^{-2})$ , the rest-frame equivalent widths  $W_r(\text{Si II } \lambda 1526)$  and  $W_r(\text{C II } \lambda 1334)$  (with non-detections indicated by “−999.00”), the measured difference,  $\Delta\beta$ , between the DLA quasar’s  $\beta$  and the mean  $\beta$  of its control distribution, the corresponding colour excess,  $E(B-V)$ , for SMC and LMC-like dust, and the number of control quasars ( $N_{\text{ctrl}}$ ). The full table is available in the electronic version of this paper (see the Supporting Information).

SDSS name (J2000)	$z_{\text{em}}$	$z_{\text{min}}$	$z_{\text{max}}$	$\beta$	$\sigma_\beta$	$\beta_{\text{nw}}$	$z_{\text{abs}}$	$N_{\text{H I}}$	$W_r [\text{\AA}]$		$\Delta\beta$	$E(B-V) [\text{mag}]$		$N_{\text{ctrl}}$
									Si II $\lambda 1526$	C II $\lambda 1334$		SMC	LMC	
001240.57+135236.7	3.1866	2.371	3.116	−1.266	0.104	−1.273	3.022	20.86	−999.00	−999.00	0.195	0.0130	0.0184	497
001328.20+135828.0	3.5755	2.501	3.499	−1.371	0.060	−1.389	3.281	21.56	0.30	0.34	0.073	0.0051	0.0078	160
001813.89+142455.6	4.2355	3.409	4.147	−1.672	0.170	−1.184	3.861	20.65	−999.00	−999.00	−0.162	−0.0110	−0.0166	29
003501.88−091817.6	2.4187	2.224	2.361	−1.608	0.080	−1.601	2.337	20.42	−999.00	−999.00	−0.063	−0.0041	−0.0059	545
005319.20+134708.8	2.9203	2.275	2.855	−1.332	0.077	−1.332	2.628	20.92	−999.00	0.62	0.146	0.0107	0.0175	352

**Table 2.** The absorber quasar sample (1069 quasars). The columns are defined in the caption of Table 1 and the full table is available in the electronic version of this paper (see the Supporting Information).

SDSS name (J2000)	$z_{\text{em}}$	$z_{\text{min}}$	$z_{\text{max}}$	$\beta$	$\sigma_\beta$	$\beta_{\text{nw}}$	$z_{\text{abs}}$	$N_{\text{H I}}$	$W_r [\text{\AA}]$		$\Delta\beta$	$E(B-V) [\text{mag}]$		$N_{\text{ctrl}}$
									Si II $\lambda 1526$	C II $\lambda 1334$		SMC	LMC	
001240.57+135236.7	3.1866	2.371	3.116	−1.266	0.104	−1.273	3.022	20.86	−999.00	−999.00	0.196	0.0125	0.0176	457
001328.20+135828.0	3.5755	2.501	3.499	−1.371	0.060	−1.389	3.281	21.56	0.30	0.34	0.091	0.0062	0.0092	140
001813.89+142455.6	4.2355	3.409	4.147	−1.672	0.170	−1.184	3.861	20.65	−999.00	−999.00	−0.214	−0.0162	−0.0261	26
003126.79+150739.5	4.2832	3.432	4.195	−2.904	0.156	−2.427	4.083	20.28	−999.00	−999.00	−1.512	−0.0984	−0.1367	31
003501.88−091817.6	2.4187	2.224	2.361	−1.608	0.080	−1.601	2.337	20.42	−999.00	−999.00	−0.063	−0.0043	−0.0062	538

**Table 3.** The non-DLA quasar sample (7105 quasars). The columns are defined in the caption of Table 1 and the full table is available in the electronic version of this paper (see the Supporting Information).

SDSS name (J2000)	$z_{\text{em}}$	$z_{\text{min}}$	$z_{\text{max}}$	$\beta$	$\sigma_\beta$	$\beta_{\text{nw}}$
000050.60−102155.9	2.6404	2.136	2.579	−2.056	0.045	−2.018
000143.41+152021.4	2.6383	2.152	2.578	−1.150	0.069	−1.158
000221.11+002149.3	3.0699	2.136	3.001	−1.422	0.053	−1.428
000300.34+160027.6	3.6983	3.545	3.619	−1.496	0.145	−1.088
000413.64−085529.6	2.4241	2.153	2.366	−1.300	0.037	−1.323

**Table 4.** The non-absorber quasar sample (6733 quasars). The columns are defined in the caption of Table 1 and the full table is available in the electronic version of this paper (see the Supporting Information).

SDSS name (J2000)	$z_{\text{em}}$	$z_{\text{min}}$	$z_{\text{max}}$	$\beta$	$\sigma_\beta$	$\beta_{\text{nw}}$
000050.60−102155.9	2.6404	2.136	2.579	−2.056	0.045	−2.018
000143.41+152021.4	2.6383	2.152	2.578	−1.150	0.069	−1.158
000221.11+002149.3	3.0699	2.136	3.001	−1.422	0.053	−1.428
000300.34+160027.6	3.6983	3.545	3.619	−1.496	0.145	−1.088
000413.64−085529.6	2.4241	2.153	2.366	−1.300	0.037	−1.323

While the SDSS spectral resolving power ( $R \approx 1800$ ) and the CNR and SNR thresholds ensure that most DLAs are identified, they are not optimal for accurately estimating  $N_{\text{H I}}$ . To cross-check our main results against different approaches to estimating  $N_{\text{H I}}$  we used the alternative, al-

beit smaller sample of DLAs from DR5 by Prochaska & Wolfe (2009); it provides results consistent with those presented here. Although their DLA search employed similar SNR threshold criteria to Noterdaeme et al. (2009b), their approach to fitting the DLAs to estimate  $N_{\text{H I}}$  differs, so we expect that a comparison of results from the two samples is a reasonable test for biases, particularly at low  $N_{\text{H I}}$ . Using the ‘statistical sample’ from Prochaska & Wolfe (2009), and a similar series of exclusions as we applied above to the Noterdaeme et al. (2009b) sample, left 526 DLA quasars and 7712 non-DLA quasars.

### 2.3 Control samples

From the non-DLA samples above (Section 2.2), a sample of “control” quasars is selected for *each* DLA quasar to benchmark the typical distribution of quasar spectral indices expected in the absence of strong absorbers. To be selected as a control quasar for a given DLA quasar with redshift  $z_{\text{em}}^{\text{DLA}}$  and DLA redshift  $z_{\text{abs}}^{\text{DLA}}$ , a non-DLA quasar with redshift  $z_{\text{em}}$  must satisfy the following criteria:

$$z_{\text{em}}^{\text{DLA}} - 0.05 \leq z_{\text{em}} \leq z_{\text{em}}^{\text{DLA}} + 0.05; \text{ and} \quad (2)$$

$$z_{\text{min}} \leq z_{\text{abs}}^{\text{DLA}} \leq z_{\text{max}}. \quad (3)$$

Here,  $z_{\text{min}}$  and  $z_{\text{max}}$  define, respectively, the minimum and maximum redshifts between which the non-DLA quasar spectrum was searched for DLAs by Noterdaeme et al. (2009b). These values were kindly provided to us by P. Noterdaeme. The maximum redshift,  $z_{\text{max}}$ , was defined for all quasars to be  $5000 \text{ km s}^{-1}$  bluewards of  $z_{\text{em}}$  so as to avoid strong absorbers associated with the quasars themselves.



This means that both the DLA and non-DLA samples defined above may have such “associated” DLAs and sub-DLAs in their spectra. However, again, this will occur with very similar frequency in both the DLA and non-DLA samples, so the differential reddening measurement will not be significantly affected. Similar criteria are applied when forming the control samples for absorber quasars from the non-absorber sample. The minimum redshift,  $z_{\min}$ , was defined by [Noterdaeme et al.](#) according to the CNR and SNR criteria mentioned in Section 2.2. This means that  $z_{\min}$  effectively acts as a spectral quality control measure to ensure that DLAs can be securely identified between  $z_{\min}$  and  $z_{\max}$ .

The first criterion above reflects the requirement for control quasars to have similar redshifts as their corresponding DLA quasar. It defines a small redshift interval within which we assume the complicated, redshift-dependent SDSS quasar selection biases are relatively constant. It effectively determines the number of control quasars for a given DLA quasar; increasing it increases the control sample size but risks larger effects from non-uniformities in the quasar selection. Reducing it substantially below  $\pm 0.05$  decreases the control samples of many DLA quasars. We find that our results are insensitive to changes in this interval up to  $\pm 0.2$ .

The second criterion above states that a non-DLA quasar can only qualify as a control quasar for a given DLA quasar (with a DLA at  $z_{\text{abs}}$ ) if a hypothetical DLA at  $z_{\text{abs}}$  could have been found within its spectrum. For that to be true,  $z_{\text{abs}}$  must lie between the  $z_{\min}$  and  $z_{\max}$  values of the non-DLA quasar. Inherent in this criterion is the assumption that DLA dust extinction and reddening are small: if they were large, and such a dusty DLA was placed between  $z_{\min}$  and  $z_{\max}$  in a non-DLA spectrum, it would suppress the continuum flux in the Ly- $\alpha$  forest region, and  $z_{\min}$  would increase, potentially to the point where the second criterion is no longer satisfied. In this sense, the CNR and SNR thresholds in the DLA search algorithm, combined with the second criterion above, may slightly diminish the measured DLA dust reddening signal compared to its true strength. However, the bias will reduce in proportion to the reddening itself, and will likely be negligible at the very small reddening levels observed in our work. Simple tests, in which  $z_{\min}$  was artificially varied for the DLA sample, confirmed this expectation.

For the statistical quasar reddening analysis below in Section 3, each DLA quasar was conservatively required to have at least 50 control quasars. This excludes 54 DLA quasars and 78 absorber quasars from the baseline samples of 774 and 1069 defined above. Figure 1 shows the resulting range in control sample sizes for the DLA quasars as a function of redshift. The median number of control quasars is 264 per DLA quasar but, like the DLA quasar distribution, this varies considerably with redshift. For example, we again notice the strong drop in control quasar numbers between  $z_{\text{em}} \sim 2.6$ –3.0 because of the similarity between quasar and stellar colours there. Note that many DLA quasars may share many control quasars in common.

Finally, we note that other recent SDSS DLA reddening studies (e.g. [Vladilo et al. 2008](#); [Frank & Péroux 2010](#); [Khare et al. 2012](#)) imposed an explicit magnitude restriction on control quasars: they required that a control quasar have a similar  $i$ -band magnitude to the corresponding DLA quasar magnitude. We do not impose such a criterion in our anal-

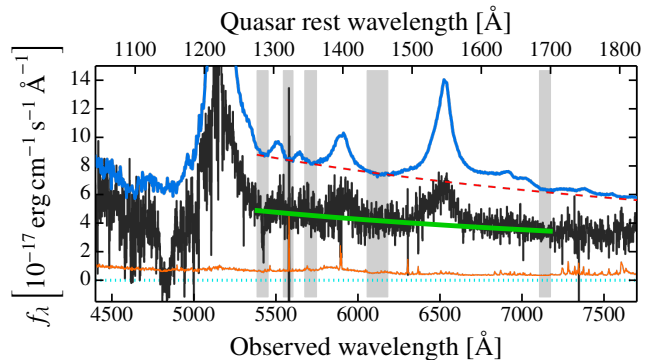


**Figure 2.** Example of spectral index fitting on the SDSS spectrum (black/dark solid line) of quasar J112820.20+325918.9 ( $z_{\text{em}} = 3.22$ ) which has a DLA at  $z_{\text{abs}} = 2.909$  with  $\log(N_{\text{H I}}/\text{cm}^{-2}) = 20.6$  ([Noterdaeme et al. 2009b](#)). The power-law (green/grey thick line) was fitted to the median fluxes within the grey shaded regions and has a spectral index  $\beta = -1.22$ . The orange/thin lower line is the  $1\text{-}\sigma$  flux uncertainty. The blue/upper curve shows the median composite SDSS quasar spectrum of [Vanden Berk et al. \(2001\)](#) and their power-law estimate of the underlying continuum (dashed line,  $\beta = -1.56$ ). Note that the grey shaded fitting regions are chosen to match areas of little or no quasar line emission.

ysis, though we emphasise that the second criterion above ensures that control quasars have the same CNR distribution in the Lyman- $\alpha$  forest region as the DLA quasars at the same redshift. We discuss the implications of matching the DLA and control quasar  $i$ -band magnitudes in Section 6.

### 3 STATISTICAL QUASAR REDDENING ANALYSIS

The spectral index,  $\beta$  in equation (1), was determined for each DLA quasar and all its control quasars following a similar approach to [Murphy & Liske \(2004\)](#), as illustrated in Fig. 2. Before performing the spectral fitting below, all quasar spectra were first corrected for Galactic extinction using the dust map of [Schlegel et al. \(1998\)](#) and the Milky Way extinction law of [O’Donnell \(1994\)](#) (based on that of [Cardelli et al. 1989](#)).

For each quasar, the median flux density was determined in 5 small spectral regions (grey shaded regions in Fig. 2) at quasar rest-frame wavelengths of 1276–1292, 1314–1328, 1345–1362, 1435–1465, 1684–1700 Å. As shown in Fig. 2, the composite SDSS spectrum of [Vanden Berk et al. \(2001\)](#) in these regions shows little or no evidence for contamination from quasar line emission and is consistent with representing the underlying power-law quasar continuum. Using the median  $f_{\lambda}$  value in each region provides robustness against the effects of narrow absorption features, bad pixels, residuals from the removal of telluric features and/or other narrow artefacts. The second region (1314–1328 Å) is the narrowest, but still comprises 47 SDSS pixels ( $69 \text{ km s}^{-1} \text{ pix}^{-1}$ ), so the median is substantially effective in guarding against these effects. As a measure of the relative uncertainty in the median fluxes, we also calculate the semi-interquartile range, i.e. half the range around the median containing half of the  $f_{\lambda}$  values, in each region. These

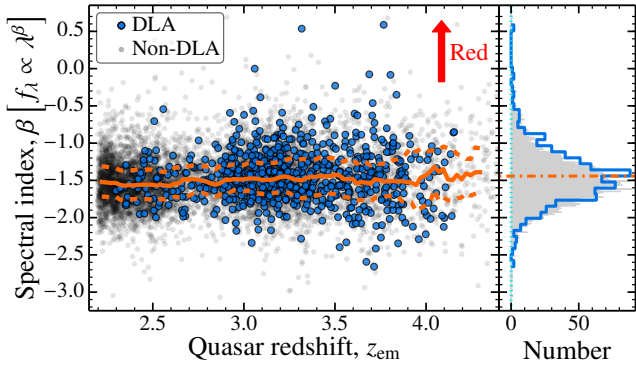


**Figure 3.** Distribution of spectral index,  $\beta$ , for the DLA quasars (dark, circled points) and non-DLA quasars (light grey points) with emission redshift. The DLA distribution clearly follows the shape of the non-DLA distribution closely. A running median (over 201 quasars) of the non-DLA quasar  $\beta$  values is plotted as an orange/grey solid line and shows some evolution with redshift (the dashed lines mark the running upper and lower quartiles). The overall  $\beta$  distributions are shown in the histograms (right-hand panel). The two distributions are similar and both display a skew towards redder  $\beta$  values. The dot-dashed line shows the mean  $\beta$  for the DLA quasars.

will be small for high SNR spectra and larger for low SNR spectra and/or regions that contain some features/artefacts extending over more than  $\sim 10$  pixels.

We estimated  $\beta$  using a weighted power-law fit to these median  $f_\lambda$  values with the inverse-squares of their semi-interquartile ranges as weights. This provides a robust, naturally-weighted  $\beta$  estimate with a representative uncertainty,  $\delta\beta$ . These uncertainties have a median of 0.13, with semi-interquartile range of 0.05 and no strong redshift dependence. Figure 3 shows the distribution of  $\beta$  with redshift for the DLA quasars and non-DLA quasars (the latter is the pool from which control quasars are selected). Note that  $\beta$  evolves little with redshift in the DR7 quasar spectra. Relative to the  $\beta$  distribution of the non-DLA quasars, there appears to be a small shift in the DLA quasar  $\beta$  distribution to redder colours at most redshifts. This is an indication that the DLAs cause their quasars to be reddened with respect to non-DLA quasars at similar redshifts (whose spectra had sufficient SNR for those DLAs to be detected). The reddening effect is substantially smaller than the width of the  $\beta$  distribution itself, highlighting the need for large statistical samples of both DLA and non-DLA quasars.

One potential concern with our spectral fitting procedure is that the relative weights of the different fitting regions will change with redshift. In particular, the redder fitting regions will move into noisier parts of the spectrum at higher redshifts, so they will contribute less to the weighted power-law fit to determine  $\beta$ . In principle, this may introduce a redshift-dependency in the spectral index results. To check this we determined the spectral index with an unweighted fit,  $\beta_{\text{unweighted}}$ , and analysed the difference,  $\beta - \beta_{\text{unweighted}}$ , for DLA quasars and non-DLA quasars as a function of redshift. There is no significant difference between the weighted and unweighted  $\beta$  values up to  $z_{\text{em}} \approx 3.3$ , but above this redshift  $\beta$  is smaller than  $\beta_{\text{unweighted}}$  by  $\approx 0.1$  on average. However, most importantly, this behaviour is the same for both the

DLA and non-DLA samples, i.e. there is no significant *differential* changes between the DLA quasar and non-DLA quasar samples with redshift. It is important to realise that variations in  $\beta$  – either real or spurious – over redshift intervals greater than the  $\Delta z = 0.1$  bin size for selecting control quasars, will not affect the  $\Delta\beta$  value for a given DLA quasar. We conclude that the weighted approach to determining the spectral index of each quasar spectrum is robust, at least to the precision required for the differential reddening analysis here.

If DLAs contain negligible dust, the distribution of  $\beta$  for DLA quasars and their control quasars should be indistinguishable. Significant DLA dust reddening should increase a DLA quasar’s spectral index,  $\beta_{\text{DLA}}$ , relative to the  $\beta$  distribution of its control quasars. That is, we should seek to measure

$$\Delta\beta \equiv \beta_{\text{DLA}} - \langle\beta_{\text{control}}\rangle \quad (4)$$

for each DLA using some appropriate definition of  $\langle\beta_{\text{control}}\rangle$ , a statistic representing the  $\beta$  distribution of that DLA quasar’s control sample. Figure 3 shows that the  $\beta$  distribution of non-DLA quasars is non-Gaussian and asymmetric. However, it also shows that the  $\beta_{\text{DLA}}$  distribution has a very similar shape. We therefore make the simple assumption in our analysis that the two distributions differ only by an average shift in the  $\beta$  distribution. This implies that  $\langle\beta_{\text{control}}\rangle$  in equation (4) is just the simple mean  $\beta$  of the control sample for each DLA quasar. For example, consider the limiting case of no DLA reddening:  $\beta_{\text{DLA}}$  in equation (4) is then equivalent to a single value drawn from the  $\beta_{\text{control}}$  distribution; considering many realizations of the same DLA quasar, the mean  $\Delta\beta$  will be zero only when  $\langle\beta_{\text{control}}\rangle$  is the mean  $\beta$  of the control sample. Simple Monte Carlo experiments confirm this, using a variety of underlying  $\beta$  distributions, even highly asymmetric ones, as long as statistical DLA reddening is assumed to simply shift the  $\beta$  distribution of non-DLA quasars.

The above approach allows us to measure a value of  $\Delta\beta$  for every DLA quasar, though it must be emphasised that individual  $\Delta\beta$  measurements are not particularly meaningful and that a statistical  $\Delta\beta$  distribution is needed to infer the average dust content of DLAs. One advantage of this approach is that some heavily reddened DLA quasars might be identifiable in this analysis. It also enables a simple conversion between  $\Delta\beta$  and the (physically more interesting) colour excess,  $E(B-V)$ , using different dust extinction laws (e.g. SMC and LMC) for each DLA – see below.<sup>2</sup> A more sophisticated definition of  $\langle\beta_{\text{control}}\rangle$  might incorporate the  $\beta$  uncertainties,  $\delta\beta$ , for the individual control quasars. However, this is only likely to affect the results if  $\delta\beta$  is a strong

<sup>2</sup> An alternative approach to determining the average reddening as a function of some physically interesting quantity, e.g.  $N_{\text{H I}}$ , would be to pre-define bins of  $N_{\text{H I}}$  and compare the distribution of  $\beta_{\text{DLA}}$  for DLAs in each bin with the collective, appropriately weighted  $\beta$  distribution of the relevant control quasars. This could be done, for example, with a maximum likelihood measure of the shift in  $\beta$  required to align the two distributions in each pre-defined bin. However, this would provide less flexibility and transparency in the results in Section 4 compared to our approach of defining  $\Delta\beta$  appropriately and measuring it for each DLA quasar.

function of  $\beta$ ; we do not observe such a relationship in our spectral fitting results, so we use the simple mean for  $\langle\beta_{\text{control}}\rangle$ .

Finally, for each DLA quasar, we convert the  $\Delta\beta$  measurement from equation (4) into DLA rest-frame colour excess value,  $E(B-V)_{\text{SMC}}$  for SMC-like dust. We redden and de-redden the DLA quasar spectrum with a wide range of  $E(B-V)$  values (both positive and negative, respectively), applied in the rest-frame of the DLA, and re-measure  $\beta$  for each value to establish a one-to-one relationship between  $E(B-V)$  and changes in  $\beta$ . Interpolating this relationship then allows conversion of an arbitrary  $\Delta\beta$  measurement into a  $E(B-V)_{\text{SMC}}$  value for that DLA quasar. The same approach is used to derive a colour excess value for LMC-like dust,  $E(B-V)_{\text{LMC}}$ . We use the SMC and LMC extinction laws from *Pei (1992)*, specifically the fitting formulae in their table 4) for this conversion. The previous spectral stacking analyses of SDSS DLAs have shown no significant evidence for a 2175 Å dust bump (*Frank & Péroux 2010; Khare et al. 2012*), so we do not include a Milky Way dust law in our analysis.

## 4 RESULTS

The main numerical results of this work are summarized in Table 5 and detailed in the following subsections. Correlations and linear relationships between the measured quantities – i.e.  $\Delta\beta$  and  $E(B-V)$  using SMC and LMC dust models – and  $z_{\text{abs}}$ ,  $N_{\text{H I}}$ , metal-line equivalent widths etc. are derived using the individual measurements, while binned measurements are plotted in the main figures. Because the scatter in the  $\Delta\beta$  and  $E(B-V)$  measurements is completely dominated by the underlying diversity of  $\beta$  values (see Fig. 3), the linear relationships are derived using unweighted linear least-squares fits. The 68 per cent confidence intervals for the parameters of these relationships and the binned measurements were all calculated using a simple bootstrap method:  $10^4$  bootstrap samples were formed by drawing, with replacement, random values from the observed distribution, and the distribution of the mean in the bootstrap samples provided the confidence intervals. Table 5 also presents results from Spearman rank (i.e. non-parametric) correlation tests between the parameters of interest, including the correlation coefficient,  $r$ , and probability,  $p$ , of the observed correlation being due to chance under the null hypothesis of no correlation.

### 4.1 Shift in spectral index

The upper panel of Fig. 4 shows the measurements of  $\Delta\beta$  [equation (4)] for the DLA quasars against the DLA absorption redshift. Compared to the  $\beta$  values shown in Fig. 3, it is immediately clear that there is no apparent redshift evolution in  $\Delta\beta$ . However, the distribution of  $\Delta\beta$  values, shown in the histogram, has a similar non-Gaussian, asymmetric shape as the  $\beta$  values, as expected.

The  $\Delta\beta$  distribution in Fig. 4 also shows that any DLA dust reddening causes a much smaller shift in  $\beta$  than the typical width of the distribution. Indeed, the mean  $\Delta\beta$  is only  $0.041 \pm 0.013$ , representing some evidence for very low DLA dust reddening. The bootstrap distribution indicates that  $\Delta\beta$  is  $>0$  at  $3.2\text{-}\sigma$  significance; that is, the null hypothesis of no DLA dust reddening is ruled out at 99.7 per cent confidence.

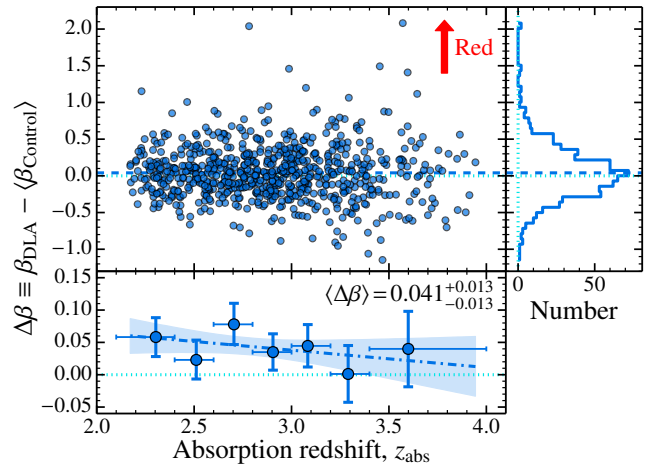


**Figure 4.** Distribution of the spectral index difference between the DLA quasars and their corresponding control quasar samples,  $\Delta\beta$  [see equation (4)]. The upper panels show the overall  $\Delta\beta$  distribution (histogram in right-hand panel) and its relationship with absorption redshift (left-hand upper panel). The dashed line shows the mean  $\Delta\beta$  value. The lower panel shows the mean  $\Delta\beta$  in absorption redshift bins (defined in Fig. 1) with 68 per cent bootstrap confidence intervals. The horizontal error bars indicate a bin’s redshift range and the point is plotted at the mean absorber redshift within the bin. The mean  $\Delta\beta$ , averaged over all redshifts (with 68 per cent confidence intervals), is also provided. The dot-dashed line is the best-fitting straight line to the individual  $\Delta\beta$  values and the shaded region shows the 68 per cent bootstrap confidence region of the fit. Despite the weak redshift evolution in  $\beta$  evident in Fig. 3, the differential analysis used to derive  $\Delta\beta$  here reveals no residual evolution in  $\Delta\beta$ .

The lower panel of Fig. 4 shows the mean  $\Delta\beta$  within the absorption redshift bins defined in Fig. 1. The binned results do not appear to reveal any evidence for evolution in  $\Delta\beta$  with redshift. Indeed, a linear least-squares fit to the individual  $\Delta\beta$  values, with bootstrap estimates of the  $1\text{-}\sigma$  parameter uncertainties, yields a best fitted relationship of  $\Delta\beta = (0.12 \pm 0.11) + z_{\text{abs}} \times (-0.03 \pm 0.04)$ , confirming this impression.

Conducting the same analysis for the absorber sample [i.e. including sub-DLAs with  $\log(N_{\text{H I}}/\text{cm}^{-2}) \geq 20.0$ ] yields a mean shift in the spectral index of  $\Delta\beta = 0.047 \pm 0.012$ , with  $\Delta\beta > 0$  at  $4.8\text{-}\sigma$  significance. That is, including the sub-DLAs somewhat increases the mean  $\Delta\beta$  and substantially increases the significance of the reddening detection. As with the DLA sample, we do not find any evidence for evolution in  $\Delta\beta$  with redshift.

### 4.2 Mean reddening and redshift evolution

Figure 5 shows the mean colour excess measurements, in the redshift bins defined in Fig. 1, after converting each DLA (and absorber) quasar’s  $\Delta\beta$  value to  $E(B-V)_{\text{SMC}}$  and  $E(B-V)_{\text{LMC}}$ , as described in Section 3. The Figures and Table 5 provide the mean  $E(B-V)$ , averaged over all redshifts, for the DLA and absorber quasar samples in both dust models. For example, assuming DLAs contain SMC-like dust, they cause a mean colour excess of  $\langle E(B-V)_{\text{SMC}} \rangle = 3.0 \pm 1.0$  mmag over the redshift range  $2 < z_{\text{abs}} < 4$ . Assuming the dust obeys an LMC-like dust law (i.e. with a shallower

**Table 5.** Main numerical results for correlation tests and linear fits between the individual  $E(B-V)$  values, measured in milli-magnitudes (mmag), and absorption redshift ( $z_{\text{abs}}$ ), neutral hydrogen column density ( $N_{\text{H I}}$ ), the Si II  $\lambda 1526$  rest-frame equivalent width [ $W_{\text{r}}(\text{Si II } \lambda 1526)$ ], the corresponding Si II metallicity ( $Z_{\text{Si}}$ ) and column density ( $N_{\text{Si II}}$ ) derived using known scaling relations (for DLAs only; see Section 4.4), and the C II equivalent width [ $W_{\text{r}}(\text{C II } \lambda 1334)$ ]. The correlations and fits are performed for both SMC and LMC-like dust models using both the DLA sample and absorber sample [which includes sub-DLAs with  $\log(N_{\text{H I}}/\text{cm}^{-2}) \geq 20.0$ ]. The first column describes the ‘model’ being tested or fitted in each row. The Spearman rank correlation coefficient,  $r$ , and associated probability,  $p$ , are provided for the correlation tests.

$E(B-V)$ [mmag] Model	DLAs: $\log(N_{\text{H I}}/\text{cm}^{-2}) \geq 20.3$		All absorbers: $\log(N_{\text{H I}}/\text{cm}^{-2}) \geq 20.0$	
	SMC dust	LMC dust	SMC dust	LMC dust
$\langle E(B-V) \rangle$	$3.0 \pm 1.0$	$6.2 \pm 2.2$	$3.6 \pm 0.9$	$7.2 \pm 1.9$
$z_{\text{abs}}$ corr. test	$r = -0.03, p = 0.35$	$r = -0.03, p = 0.40$	$r = -0.00, p = 0.99$	$r = -0.01, p = 0.87$
$a + b z_{\text{abs}}$	$a = 8.0 \pm 7.8,$ $b = -1.7 \pm 2.8$	$a = 11 \pm 19,$ $b = -1.9 \pm 7.0$	$a = 3.5 \pm 7.0,$ $b = 0.0 \pm 2.4$	$a = 5 \pm 17,$ $b = 0.7 \pm 6.2$
$N_{\text{H I}}$ corr. test	$r = 0.04, p = 0.24$	$r = 0.05, p = 0.21$	$r = 0.02, p = 0.51$	$r = 0.02, p = 0.43$
$b [N_{\text{H I}}/\text{cm}^{-2}]$	$b = (3.5 \pm 1.0) \times 10^{-21}$	$b = (7.8 \pm 2.1) \times 10^{-21}$	$b = (3.8 \pm 1.0) \times 10^{-21}$	$b = (8.3 \pm 2.1) \times 10^{-21}$
$a + b [N_{\text{H I}}/\text{cm}^{-2}]$	$a = 1.7 \pm 1.4,$ $b = (2.4 \pm 1.4) \times 10^{-21}$	$a = 2.8 \pm 3.3,$ $b = (6.0 \pm 3.1) \times 10^{-21}$	$a = 2.6 \pm 1.1,$ $b = (1.9 \pm 1.3) \times 10^{-21}$	$a = 4.6 \pm 2.4,$ $b = (4.9 \pm 2.9) \times 10^{-21}$
$W_{\text{r}}(\text{Si II } \lambda 1526)$ corr. test	$r = 0.19, p = 3.9 \times 10^{-4}$	$r = 0.19, p = 3.8 \times 10^{-4}$	$r = 0.17, p = 3.7 \times 10^{-4}$	$r = 0.17, p = 5.3 \times 10^{-4}$
$b [W_{\text{r}}(\text{Si II } \lambda 1526)/\text{\AA}]$	$b = 5.0 \pm 1.4$	$b = 9.2 \pm 3.0$	$b = 6.4 \pm 1.4$	$b = 12 \pm 3$
$a + b [W_{\text{r}}(\text{Si II } \lambda 1526)/\text{\AA}]$	$a = -3.7 \pm 2.2,$ $b = 7.8 \pm 2.2$	$a = -11 \pm 5,$ $b = 17 \pm 5$	$a = -1.8 \pm 2.2,$ $b = 7.9 \pm 2.3$	$a = -3.8 \pm 4.3,$ $b = 16 \pm 5$
$b Z_{\text{Si}}$	$b = 33 \pm 9$	$b = 65 \pm 21$		
$N_{\text{Si II}}$ corr. test	$r = 0.15, p = 4.2 \times 10^{-3}$	$r = 0.16, p = 2.7 \times 10^{-3}$		
$b [N_{\text{Si II}}/\text{cm}^{-2}]$	$b = (5.2 \pm 1.3) \times 10^{-16}$	$b = (10 \pm 3) \times 10^{-16}$		
$W_{\text{r}}(\text{C II } \lambda 1334)$ corr. test	$r = 0.16, p = 4.6 \times 10^{-3}$	$r = 0.16, p = 5.7 \times 10^{-3}$	$r = 0.12, p = 0.02$	$r = 0.11, p = 0.03$
$b [W_{\text{r}}(\text{C II } \lambda 1334)/\text{\AA}]$	$b = 3.1 \pm 1.3$	$b = 6.4 \pm 2.6$	$b = 3.9 \pm 1.5$	$b = 6.7 \pm 2.7$
$a + b [W_{\text{r}}(\text{C II } \lambda 1334)/\text{\AA}]$	$a = -4.2 \pm 2.3,$ $b = 6.0 \pm 2.3$	$a = -9.4 \pm 4.8,$ $b = 13 \pm 4$	$a = -2.8 \pm 2.4,$ $b = 5.9 \pm 2.5$	$a = -6.5 \pm 5.0,$ $b = 11 \pm 5$

extinction curve), the corresponding mean colour excess is higher,  $\langle E(B-V)_{\text{LMC}} \rangle = 6.2 \pm 2.2$  mmag. The overall evidence for  $E(B-V) > 0$  is, of course, very similar to that for  $\Delta\beta > 0$ : 3.2- $\sigma$  significance, averaged over all redshifts, for both SMC and LMC-like dust.

Table 5 shows that both the colour excess and statistical significance of  $E(B-V)$  increase when sub-DLAs with  $\log(N_{\text{H I}}/\text{cm}^{-2}) \geq 20.0$  are included (as also seen for  $\Delta\beta$ ). In both dust models,  $E(B-V) = 0$  is ruled out at 4.8- $\sigma$  significance.

Figure 5 reveals no evidence for redshift evolution in the colour excess caused by dust in DLAs and sub-DLAs. The bootstrap uncertainty in the (assumed) linear relationship between  $E(B-V)$  and  $z_{\text{abs}}$  is illustrated by the shaded regions in the Figures; these are all clearly consistent with no evolution in  $E(B-V)$ . The best-fit parameter values and uncertainties are provided in Table 5. For example, the 1- $\sigma$  limit on evolution in  $E(B-V)_{\text{SMC}}$  is 2.8 mmag per unit redshift for DLAs, assuming an SMC-like dust model, and a similar value, 2.4 mmag per redshift interval, when including sub-DLAs. The lack of redshift evolution is also confirmed in Table 5 with the Spearman rank tests for correlations. These return  $p$  values  $> 35$  per cent in all four cases (DLA and absorber samples with SMC and LMC-like dust), indicating no significant correlation between  $E(B-V)$  and  $z_{\text{abs}}$ . Over the same redshift interval,  $z_{\text{abs}} = 4-2$ , the mean DLA metallicity has been found to increase by a factor of  $\approx 2.5$  (Rafelski et al. 2012; Jorgenson et al. 2013). If the mean dust column scales linearly with DLA metallicity, as expected in

simple models (e.g. Vladilo & Péroux 2005), we should expect a slope of  $b \approx 1.3$  mmag per unit redshift in  $E(B-V)_{\text{SMC}}$ . However, Table 5 shows that our 1- $\sigma$  sensitivity to a slope is  $b = 2.8$  mmag per unit redshift. That is, the SDSS DLA dataset is not large enough to detect the evolution in dust content expected from the observed metallicity evolution in DLAs.

### 4.3 Reddening vs. neutral hydrogen column density

Figure 6 shows the mean colour excess measurements in bins of  $\log N_{\text{H I}}$  using the sample of all absorbers with  $\log(N_{\text{H I}}/\text{cm}^{-2}) \geq 20.0$ . Using the DLA sample returns very similar results at  $\log(N_{\text{H I}}/\text{cm}^{-2}) \geq 20.3$  but, by definition, does not extend to lower  $N_{\text{H I}}$ , so we focus on the full absorber sample here. The binned results in Fig. 6 provide no evidence for strong variations in  $E(B-V)$  with increasing  $N_{\text{H I}}$ . Nor do the Spearman rank correlation tests in Table 5 indicate significant correlation or anti-correlation ( $p > 0.2$  in all cases). It is instead notable that the amount of reddening is similar at all H I column densities over a 1.5 order-of-magnitude range and that the highest and lowest  $N_{\text{H I}}$  bins show no discernable differences.

In both the SMC and LMC, the colour excess is correlated with  $N_{\text{H I}}$ , with the reddening per H atom (including contributions from  $\text{H}_2$ ) being  $E(B-V)/N_{\text{H}} \approx 2 \times 10^{-23}$  (Martin et al. 1989) and  $\approx 4.5 \times 10^{-23}$  mag  $\text{cm}^2$  (Fitzpatrick 1985), respectively. This motivates a linear fit between our



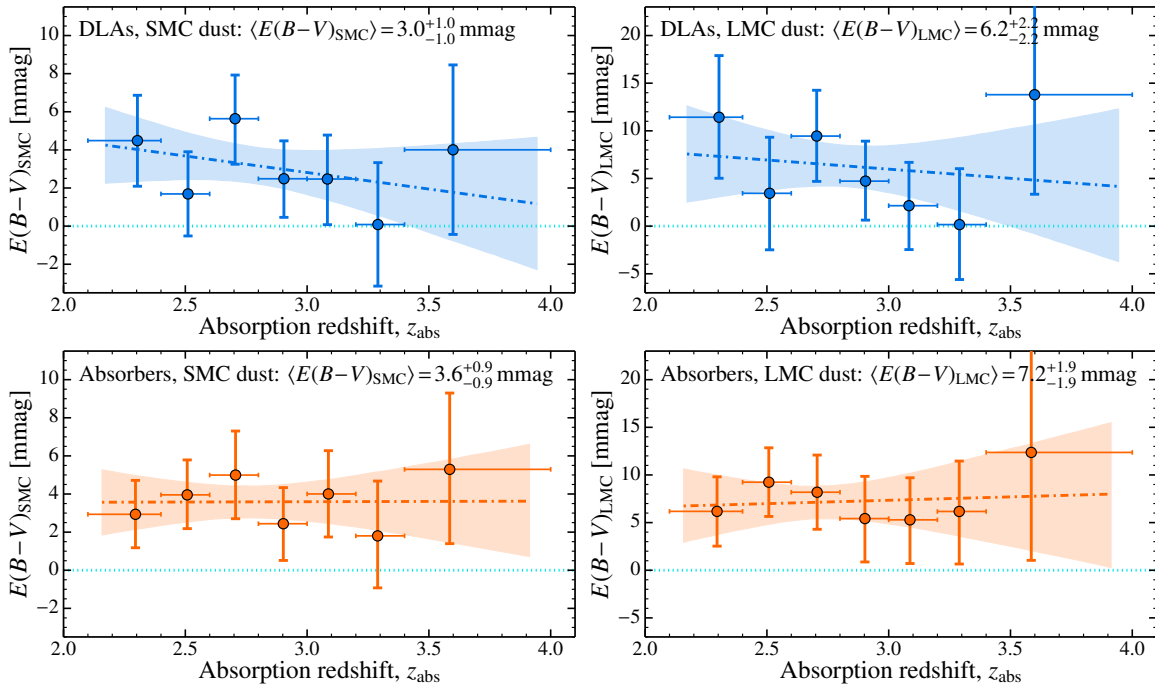


**Figure 5.** The mean colour excess,  $E(B-V)$ , in the absorber rest-frame in bins of absorption redshift (defined in Fig. 1). The upper plots show the mean  $E(B-V)_{\text{SMC}}$  (left-hand plot) and  $E(B-V)_{\text{LMC}}$  (right-hand plot) values for the DLAs, while the lower plots show the values for all absorbers with  $\log(N_{\text{H I}}/\text{cm}^{-2}) \geq 20.0$ . Note the doubled  $E(B-V)$  scale for the LMC plots. The vertical error bars represent the 68 per cent bootstrap confidence intervals. The horizontal error bars indicate a bin's range and the point is plotted at the mean absorber redshift within the bin. The dot-dashed lines are the best-fit straight lines to the individual  $E(B-V)$  values as a function of redshift, with the 68 per cent bootstrap confidence intervals in the fits shown as shaded regions.

individual  $E(B-V)$  results and  $N_{\text{H I}}$ , as shown by the dot-dashed lines and  $1-\sigma$  shaded regions in Fig. 6. Although there is no evidence for such a relationship, as discussed above, the data in Fig. 6 are not inconsistent with the best-fit relationships derived. For better comparison with the SMC and LMC, we restricted these fits to DLAs according to the traditional threshold for selecting only the most neutral absorbers [i.e.  $\log(N_{\text{H I}}/\text{cm}^{-2}) \geq 20.3$ ]. The resulting parameter estimates are given in Table 5. Assuming a negligible  $\text{H}_2$  molecular fraction in our DLAs, the mean reddening per H atom is  $E(B-V)_{\text{SMC}}/N_{\text{H}} \approx 0.4 \times 10^{-23}$  and  $E(B-V)_{\text{LMC}}/N_{\text{H}} \approx 0.8 \times 10^{-23} \text{ cm}^2$ . These are only  $\approx 20$  per cent of the SMC and LMC values given above.

Even if the assumption of a simple linear relationship between  $E(B-V)$  and  $N_{\text{H I}}$  is valid for DLAs, the much smaller mean reddening per H atom for DLAs is most likely explained by their much lower average metallicity of  $\sim 1/30$  solar (e.g. Rafelski et al. 2012; Jorgenson et al. 2013) compared to the SMC and LMC ( $\sim 1/7$  and  $\sim 1/3$  solar; Kurt & Dufour 1998; Draine 2003). However, while the interstellar medium within each of the Magellanic Clouds shows little metallicity variation, the DLA population exhibits a very large range,  $[M/H] \sim -3.0$ – $0.0^3$ . Therefore, even if  $E(B-V)$  correlates tightly with  $N_{\text{H I}}$  in the different regions of individ-

ual high-redshift galaxies (e.g. disk, gaseous halo etc.) with  $\log(N_{\text{H I}}/\text{cm}^{-2}) \geq 20.3$ , the large metallicity range of the DLAs – an ensemble of different regions from different galaxies – will tend to flatten any  $E(B-V)$  vs.  $N_{\text{H I}}$  correlation, possibly leading to an apparently flat relationship like those observed in Fig. 6.

#### 4.4 Reddening vs. metal line equivalent width, metallicity and metal column density

In addition to measuring  $N_{\text{H I}}$  for each DLA candidate, Noterdaeme et al. (2009b) determined the equivalent widths of several strong metal absorption lines when they fell redwards of the quasar Ly- $\alpha$  emission line. Si II  $\lambda 1526$  is the strongest Si II transition and its rest-frame equivalent width,  $W_{\text{r}}(\text{Si II } \lambda 1526)$ , was reported for 355 of the 730 DLA quasars in our statistical analysis (and 428 of the 991 absorber quasars). Similarly,  $W_{\text{r}}(\text{C II } \lambda 1334)$  was reported for 303 DLA quasars (and 373 absorber quasars). The unreported cases will be a mix of non-detections (i.e. where the metal absorption was too weak to detect) and where detection was precluded, either because the transitions fell bluewards of the quasar Ly- $\alpha$  emission line or due to some artefact in the spectra (e.g. bad pixels).

Figures 7 and 8 show the mean colour excess measurements in bins of  $W_{\text{r}}(\text{Si II } \lambda 1526)$  and  $W_{\text{r}}(\text{C II } \lambda 1334)$ , respectively. There is a clear tendency for systems with larger metal-line equivalent widths to exhibit more reddening. The correlation tests in Table 5 confirm this: for exam-

<sup>3</sup> We use the standard notation for metallicity, with  $[M/H] \equiv \log[N(M)/N(H)] - \log[N(M)/N(H)]_{\odot}$  and  $Z_{\text{M}} \equiv 10^{[M/H]}$ , where the solar abundance ratios,  $[N(M)/N(H)]_{\odot}$ , are taken from Asplund et al. (2009).

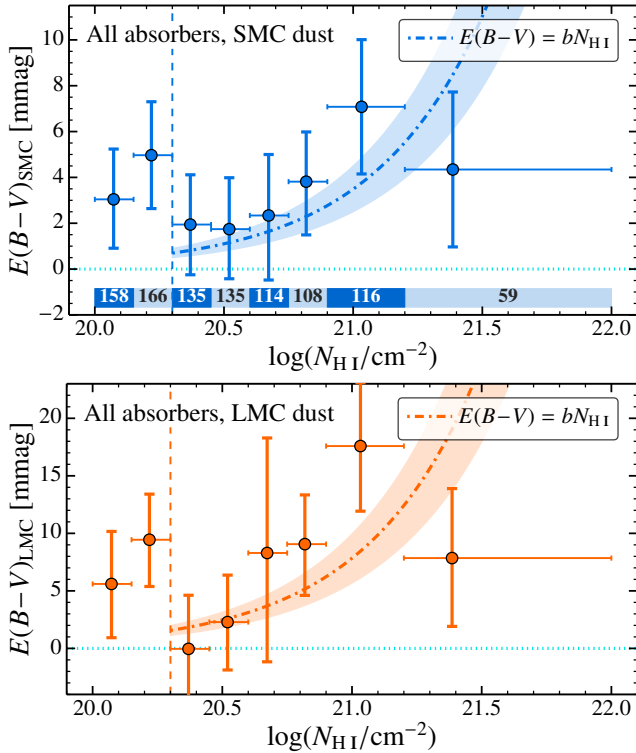


**Figure 6.** The mean colour excess,  $E(B-V)$ , in the absorber rest-frame in bins of  $\log N_{\text{HI}}$ . The upper plot shows the mean  $E(B-V)_{\text{SMC}}$  values while the lower plot shows the  $E(B-V)_{\text{LMC}}$  values. Note the doubled  $E(B-V)$  scale for the LMC plot. The shaded bar in the upper plot shows the number of absorbers in each  $\log N_{\text{HI}}$  bin. The vertical error bars represent the 68 per cent bootstrap confidence intervals. The horizontal error bars indicate a bin's range and the point is plotted at the mean  $\log N_{\text{HI}}$  within the bin. The dot-dashed lines are the best-fit straight lines to the individual  $E(B-V)$  values as a function of  $N_{\text{HI}}$  [not  $\log N_{\text{HI}}$ , hence their curvature in the plot], with the 68 per cent bootstrap confidence intervals in the fits shown as shaded regions. The dashed lines delineate DLAs and sub-DLAs. Note that the results in both plots were derived from analysing the absorber (and corresponding non-absorber) sample containing DLAs and sub-DLAs with  $\log(N_{\text{HI}}/\text{cm}^{-2}) \geq 20.0$ . The results from the DLA/non-DLA analysis are very similar for  $\log(N_{\text{HI}}/\text{cm}^{-2}) \geq 20.3$ .

ple,  $E(B-V)_{\text{SMC}}$  correlates strongly with  $W_r(\text{Si II } \lambda 1526)$  for DLAs, with the Spearman rank test giving a probability of  $p = 0.04$  per cent of the observed level of correlation occurring by chance alone, i.e. a  $\approx 3.5\sigma$  significance. The correlation is of similar strength, but lower significance ( $\approx 2.8\sigma$ ), between  $E(B-V)_{\text{SMC}}$  and  $W_r(\text{C II } \lambda 1334)$ . Figures 7 and 8 also show the best linear fits to the ensemble of  $E(B-V)$  and metal-line equivalent width measurements from individual absorbers. Table 5 provides the best-fitting parameters: for example,  $E(B-V)_{\text{SMC}} = (5.0 \pm 1.4) \times [W_r(\text{Si II } \lambda 1526)/\text{\AA}]$  mmag for DLAs.

A strong correlation between DLA dust content and metal-line column density is perhaps the most basic and assumption-free relationship we should expect (e.g. Vladilo & Péroux 2005). Given the SDSS spectral resolution of  $\sim 170 \text{ km s}^{-1}$  and the typical rest-frame equivalent width detection limits ( $\sim 0.15 \text{ \AA}$  at  $1\sigma$ ), the detected metal transitions will be predominantly saturated. Therefore, variation

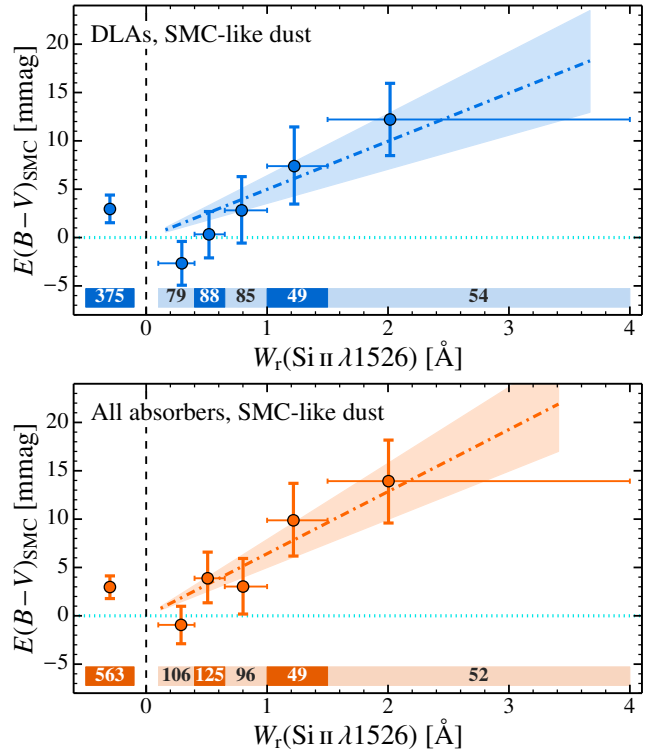


**Figure 7.** The mean colour excess for SMC-like dust,  $E(B-V)_{\text{SMC}}$ , in the absorber rest-frame in bins of  $\text{Si II } \lambda 1526$  rest equivalent width,  $W_r(\text{Si II } \lambda 1526)$ . The upper plot shows the mean  $E(B-V)_{\text{SMC}}$  values for the DLAs, while the lower plot shows the values for all absorbers with  $\log(N_{\text{HI}}/\text{cm}^{-2}) \geq 20.0$ . The shaded bar in each plot shows the number of absorbers in each bin. The left-most point in each plot is the mean  $E(B-V)$  value for DLAs/absorbers in which  $\text{Si II}$  was not detected (see main text). The vertical error bars represent the 68 per cent bootstrap confidence intervals. The horizontal error bars indicate a bin's range and the point is plotted at the mean  $W_r(\text{Si II } \lambda 1526)$  within the bin. The dot-dashed lines are the best-fit straight lines to the individual  $E(B-V)$  values as a function of  $W_r(\text{Si II } \lambda 1526)$ , with the 68 per cent bootstrap confidence intervals in the fits shown as shaded regions.

in their equivalent widths will more directly reflect variations in the total velocity width of the underlying absorption profile – i.e. the velocity spread amongst the individual  $\sim 5\text{--}10 \text{ km s}^{-1}$ -wide components – rather than the metal column densities of those individual components. Nevertheless, a broader profile will in general comprise more components, so the metal column density should correlate strongly with equivalent width. That is, we should expect the dust column density and  $E(B-V)$  to correlate strongly with  $W_r(\text{Si II } \lambda 1526)$  and  $W_r(\text{C II } \lambda 1334)$ . Therefore, the increase in  $E(B-V)$  with increasing metal-line equivalent width in Figs. 7 and 8 indicates that the mean reddening of DLA quasars we observe (Fig. 4) is really due to dust in the DLAs and not due (primarily) to some spurious, systematic effect.

Considering all absorbers with  $\log(N_{\text{HI}}/\text{cm}^{-2}) \geq 20.0$ , the correlations for  $E(B-V)$  and  $W_r(\text{Si II } \lambda 1526)$  have similar strengths and significance, and the best-fit linear relationships have similar slopes, as for DLAs (assuming either SMC or LMC-like dust). However, for  $W_r(\text{C II } \lambda 1334)$ , the correlation becomes weaker and substantially less significant: e.g. for SMC-like dust, the by-chance correlation prob-

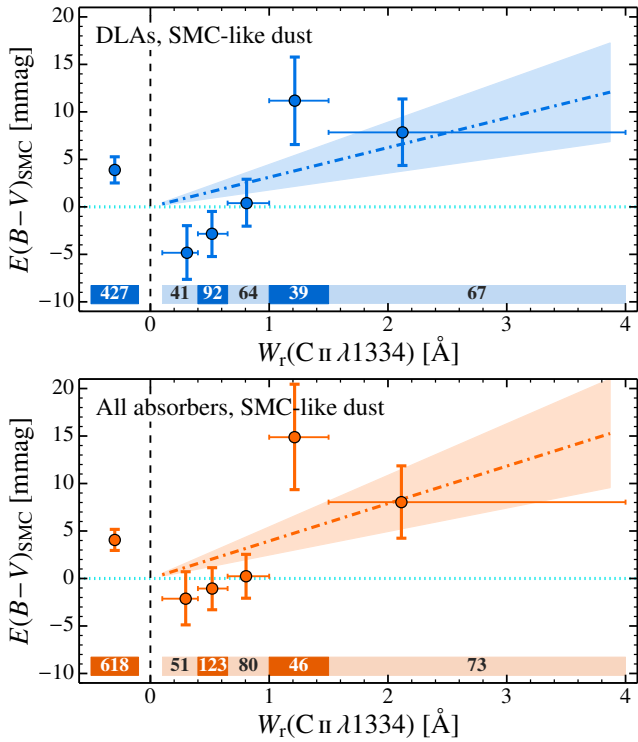


**Figure 8.** The mean colour excess for SMC-like dust,  $E(B-V)_{\text{SMC}}$ , in the absorber rest-frame in bins of  $\text{C II } \lambda 11334$  rest equivalent width,  $W_r(\text{C II } \lambda 11334)$ . The upper plot shows the mean  $E(B-V)_{\text{SMC}}$  for DLAs while the lower plot shows the values for all absorbers with  $\log(N_{\text{H I}}/\text{cm}^{-2}) \geq 20.0$ . The shaded bars show the number of absorbers in each bin. The left-most point in each plot is the mean  $E(B-V)_{\text{SMC}}$  value for DLAs/absorbers in which  $\text{C II}$  was not detected (see main text). The vertical error bars represent the 68 per cent bootstrap confidence intervals. The horizontal error bars indicate a bin's range and the point is plotted at the mean  $W_r(\text{C II } \lambda 11334)$  within the bin. The dot-dashed lines are the best-fit straight lines to the individual  $E(B-V)_{\text{SMC}}$  values as a function of  $W_r(\text{C II } \lambda 11334)$ , with the 68 per cent bootstrap confidence intervals in the fits shown as shaded regions.

ability between  $E(B-V)_{\text{SMC}}$  and  $W_r(\text{C II } \lambda 11334)$  increases from  $p = 0.5$  per cent for the 303 DLA quasars to 2 per cent for the 373 absorber quasars. Comparison of the upper and lower panels of Fig. 8, which show the  $E(B-V)_{\text{SMC}}-W_r(\text{C II } \lambda 11334)$  relationships for DLA and absorber quasars, indicates that the main difference is at low values of  $W_r(\text{C II } \lambda 11334)$ : for DLA quasars the two lowest- $W_r(\text{C II } \lambda 11334)$  bins lie  $\approx 1.1$  and  $1.7\sigma$  below zero reddening, while for the absorber quasars they are closer to zero. That is, the strength of the  $E(B-V)-W_r(\text{C II } \lambda 11334)$  correlation for DLAs may be overestimated in the DLA and absorber quasar samples. While the deviation of  $E(B-V)$  below zero at low  $W_r(\text{C II } \lambda 11334)$  is consistent with a statistical fluctuation, it may indicate that we generally underestimate  $E(B-V)$  in our sample. We consider one possible systematic effect that could, in principle, cause this – the SDSS colour-selection algorithm for selecting quasars for spectroscopic follow-up – in Section 5, though we conclude there that it causes  $<5$  per cent bias at all redshifts in our samples.

The equivalent width of  $\text{Si II } \lambda 1526$  is also particularly interesting because it has been found to correlate very

strongly with DLA metallicity,  $[\text{M}/\text{H}]$ , with only a  $\sim 0.25$  dex scatter and a linear relationship as follows (Prochaska et al. 2008):

$$[\text{M}/\text{H}] = (-0.92 \pm 0.05) + (1.41 \pm 0.10) \log_{10}[W_r(\text{Si II } \lambda 1526)/\text{\AA}]. \quad (5)$$

Similarly tight and strong relationships were also reported by Kaplan et al. (2010), Neelaman et al. (2013) and Jorgenson et al. (2013). The upper panel of Fig. 9 shows the result of converting  $W_r(\text{Si II } \lambda 1526)$  to metallicity using equation (5) for the DLAs and the linear fit between  $E(B-V)_{\text{SMC}}$  and  $W_r(\text{Si II } \lambda 1526)$  from Fig. 7's upper panel. Table 5 also shows the results for the best linear fits between the ensemble of  $E(B-V)$  values for DLAs and  $Z_{\text{Si}} \equiv 10^{[\text{M}/\text{H}]}$  derived using equation (5); for example,  $E(B-V)_{\text{SMC}} = (33 \pm 9) Z_{\text{Si}}$  mmag. By comparison, assuming that  $E(B-V)$  is instead linearly proportional to  $W_r(\text{Si II } \lambda 1526)$ , equation (5) implies that  $E(B-V)$  should be proportional to  $Z_{\text{Si}}^{1/1.41}$ ; for example, from the fitting results in Table 5 for SMC-like dust in DLAs, the relationship would be  $E(B-V)_{\text{SMC}} = (23 \pm 6) Z_{\text{Si}}^{1/1.41}$  mmag. While both relationships appear to reasonably reflect the underlying trend between  $E(B-V)$  and metal-line equivalent width and/or metallicity that we observe, the significant scatter in our  $E(B-V)$  values clearly prevents us from assessing which relationship is a more accurate description.

The lower panel of Fig. 9 shows the result of converting  $W_r(\text{Si II } \lambda 1526)$  to a  $\text{Si II}$  column density using equation (5) and the neutral hydrogen column density for each DLA, i.e.  $N_{\text{Si II}} = 10^{-0.92} [N_{\text{Si II}}/N_{\text{H I}}]_{\odot} W_r(\text{Si II } \lambda 1526)^{1.41} N_{\text{H I}}$ . Table 5 shows that, while a correlation between  $E(B-V)$  and  $N_{\text{Si II}}$  is apparent, the statistical significance is lower than that between  $E(B-V)$  and  $W_r(\text{Si II } \lambda 1526)$ . For example,  $E(B-V)_{\text{SMC}}$  is correlated with  $W_r(\text{Si II } \lambda 1526)$  at  $\approx 3.5\sigma$  but only at  $\approx 2.8\sigma$  with the values of  $N_{\text{Si II}}$  derived in this way. This is likely due to the lack of any strong correlation between  $E(B-V)$  and  $N_{\text{H I}}$  in our sample (see Fig. 6 and Table 5). The best-fitted linear relationship between the individual  $E(B-V)$  measurements and the  $N_{\text{Si II}}$  values is provided in Table 5 and, for SMC-like dust in DLAs, plotted in Fig. 9. The reduced significance of the correlation is apparent, with a larger scatter around the best-fit relationship observed here compared to, e.g., the relationship with  $[\text{M}/\text{H}]$  in the upper panel.

## 5 MAGNITUDE AND COLOUR SELECTION BIASES

Dust in DLAs will cause both extinction and reddening of DLA quasars. Therefore, it is important to address the possible effect that the magnitude and colour-selection criteria of SDSS quasars (Richards et al. 2002) may have on the measured reddening signal. Dusty DLAs may be preferentially selected or rejected, with the degree of bias varying with redshift. This possibility has not been thoroughly addressed in previous SDSS DLA reddening studies, possibly because the selection algorithm is very complex and not available in portable, public software. The colour-selection criteria are highly redshift-dependent, especially around redshifts where optical quasar colours are very similar to stellar colours,  $z_{\text{em}} \sim 2.5-3.0$ , which is especially concerning for reddening studies of DLAs. The magnitude selection criterion for most SDSS quasar candidates ( $i \leq 19.1$  mag) is, by comparison, relatively simple and, being applied in the  $i$ -band, will be

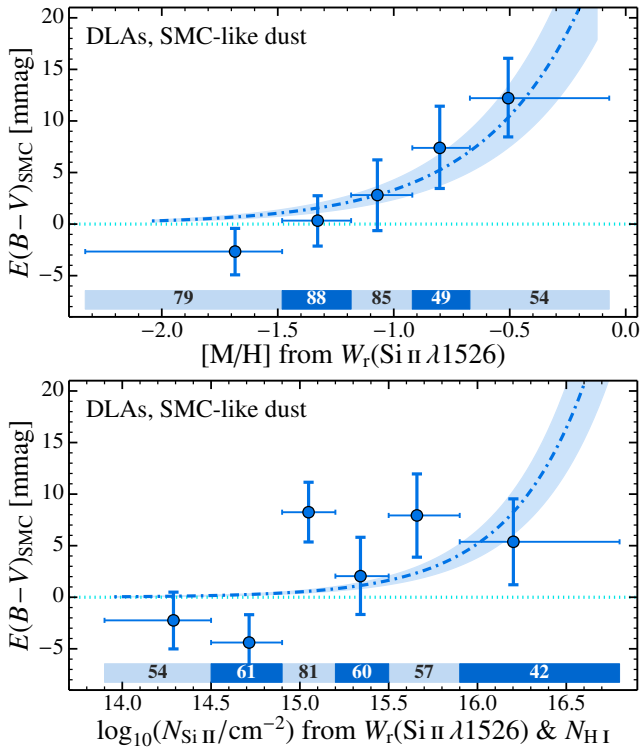


**Figure 9.** Relationship between mean colour-excess for SMC-like dust in DLAs and the metallicity,  $[M/H]$ , and Si II column density,  $N_{\text{Si II}}$ , inferred from  $W_r(\text{Si II } \lambda 1526)$  and  $N_{\text{H I}}$ . The upper panel shows  $E(B-V)_{\text{SMC}}$  in bins of  $[M/H]$  and the best-fitted linear relationship between  $E(B-V)_{\text{SMC}}$  and  $W_r(\text{Si II } \lambda 1526)$  (dot-dashed line), both converted to metallicity using the known, tight correlation between  $W_r(\text{Si II } \lambda 1526)$  and  $[M/H]$  in DLAs in equation (5). The shaded bars show the number of absorbers in each bin. DLAs for which  $W_r(\text{Si II } \lambda 1526)$  was not reported by Noterdaeme et al. (2009b) are excluded. The vertical error bars represent the 68 per cent bootstrap confidence intervals. The horizontal error bars indicate a bin's range and the point is plotted at the mean  $[M/H]$  within the bin. The lower panel shows the same information for bins of  $N_{\text{Si II}}$  derived from  $W_r(\text{Si II } \lambda 1526)$  using equation (5) and the  $N_{\text{H I}}$  value for each DLA. The dot-dashed line shows the best-fit straight line to the individual  $E(B-V)_{\text{SMC}}$  values as a function of  $N_{\text{Si II}}$ , with the 68 per cent bootstrap confidence interval in the fit shown as a shaded region.

less affected by dust extinction than the bluer  $u$ ,  $g$  and  $r$  bands. However, the effect of dust on the  $i$ -band magnitude will increase as the absorber redshift increases. Further, a fainter magnitude criterion of  $i < 20.2$  mag was applied to candidates which, from the photometric colours, indicated the quasar was likely at high redshift,  $z_{\text{em}} > 3.0$ .

To address this concern and test the potential biases on our  $E(B-V)$  measurements, we have emulated the selection criteria for spectroscopic follow-up of SDSS quasar candidates detailed by Richards et al. (2002). Our implementation and some basic performance tests are described in Appendix A, and the code is made publicly available in a portable form in Bernet & Murphy (2015). While we hope this code has broad usefulness, we emphasise that it has been tested mainly for its purpose in the current analysis; we encourage other researchers to test it for their specific purposes. We also note that there exist several additional,

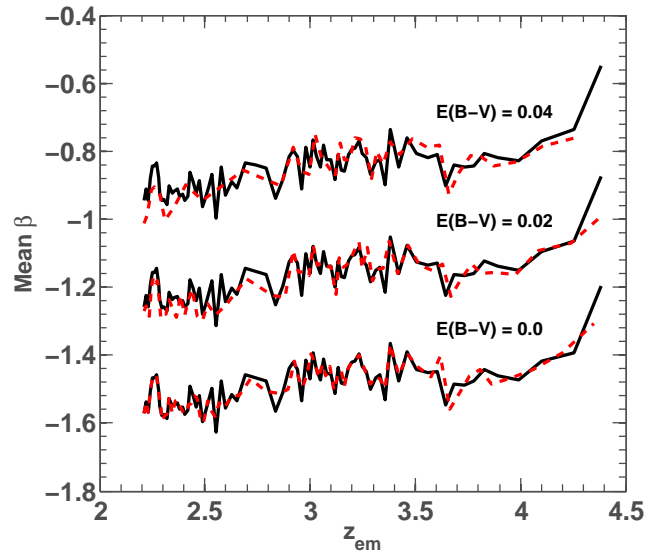


**Figure 10.** Mean spectral index,  $\beta$ , in bins containing 100 quasars, as a function of emission redshift,  $z_{\text{em}}$ , for the 7929 quasars in the Noterdaeme et al. (2009b) sample falling in the relevant redshift range ( $2.2 \leq z_{\text{em}} \leq 4.42$ ). The black solid lines show the mean  $\beta$  for the original sample [i.e.  $E(B-V)_{\text{SMC}} = 0$  mag] and where each quasar spectrum was reddened with  $E(B-V)_{\text{SMC}} = 0.02$  and  $0.04$  mag. The red dashed lines show the mean  $\beta$  of the reduced samples after passing the appropriately reddened photometry through our emulation of the SDSS quasar selection algorithm in Appendix A.

practical criteria that determined whether a specific quasar candidate was followed-up spectroscopically that are not reflected in our algorithm at all. For example, “fibre collisions” between quasar candidates and higher-priority targets for the SDSS (e.g. low- $z$  galaxies) may mean that a specific quasar candidate that passed the magnitude and colour-selection criteria was not observed in reality. In this respect, our emulation of the quasar selection algorithm should only be used in a statistical way.

With the quasar selection algorithm in hand, we can artificially dust-redden each quasar spectrum, with a certain  $E(B-V)$ , and then check whether they are selected by the quasar algorithm. This approach enables the simple test shown in Fig. 10. Here we use the entire sample of quasars in the Noterdaeme et al. (2009b) catalogue which fall in the relevant redshift range for our study,  $2.2 \leq z_{\text{em}} \leq 4.42$ . This provides a 10-times larger sample than, say, applying the test to just the DLA quasar sample alone. Three different SMC-like reddening values [ $E(B-V)_{\text{SMC}} = 0, 0.02$  and  $0.04$  mag] are applied, at the emission redshift, to each quasar’s photometry and spectrum, and the resulting  $ugriz$  magnitudes are passed through our selection code. Figure 10 compares the mean spectral index,  $\beta$  (determined as in Section 3), as a function of emission redshift in bins containing 100 quasars, both before (black line) and after (dashed red line) the selection code is applied.

Firstly, Fig. 10 demonstrates the simple, expected result that reddening the spectra by an increment of  $E(B-V)_{\text{SMC}} = 0.02$  mag increases the mean  $\beta$  by  $\sim 0.3$  over the whole redshift range. Secondly, focussing on the zero-reddening case, note



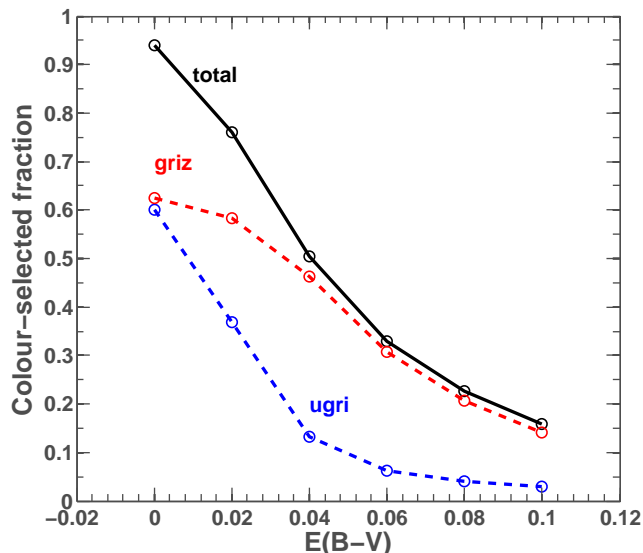


**Figure 11.** Fraction of quasars passing the magnitude and colour selection criteria (“colour-selected fraction”) in our emulated SDSS algorithm (Appendix A) as a function of the artificial reddening applied,  $E(B-V)_{\text{SMC}}$  (at the quasar emission redshift), to the photometry. The blue (lower) and red (higher) dashed lines correspond to quasar selected via the *ugri* (typically  $z_{\text{em}} < 3.0$ ) and *griz* (typically  $z_{\text{em}} > 3.0$ ) channels, whereas the “total” (black solid line) corresponds to those selected via either the *ugri* or *griz* channels. See Appendix A for further details.

that the after-selection curve (red dashed line) does not completely match the before-selection curve (black line). This is because not all quasars in the [Noterdaeme et al. \(2009b\)](#) catalogue are colour-selected;  $\approx 9$  per cent of the SDSS DR7 quasars were selected by other criteria, such as radio loudness or X-ray emission ([Schneider et al. 2010](#)). Figure 11 shows the fraction of quasars that pass the magnitude and colour-selection criteria in our code – which we refer to as the “colour-selected fraction” for brevity – is a function of  $E(B-V)_{\text{SMC}}$ . The colour-selected fraction at zero reddening is similar to that expected, and the fraction remaining at  $E(B-V)_{\text{SMC}} = 0.003$  mag – the mean value we find for SDSS DLAs – is just  $\approx 2$  per cent lower than at zero reddening. Nevertheless, the fraction drops very quickly with increased reddening, and just  $\approx 52$  per cent remain if a reddening of  $E(B-V)_{\text{SMC}} = 0.04$  mag is applied. See Appendix A for a description of the channels through which a quasar can escape the magnitude and colour-selection criteria.

Finally and most importantly, Fig. 10 clearly demonstrates that, despite the  $\sim 50$  per cent decrease in the colour-selected fraction at  $E(B-V)_{\text{SMC}} = 0.04$  mag, the mean  $\beta$  is almost unaffected and, at all redshifts, is very similar to the mean  $\beta$  before the magnitude and colour-selection criteria are applied. Indeed, the difference between the before- and after-selection curves for the  $E(B-V)_{\text{SMC}} = 0.04$  mag case is  $< 5$  per cent of the absolute shift in mean  $\beta$  (i.e. from the zero-reddening case). The largest effects are only seen at the lowest and highest redshifts ( $z_{\text{em}} \lesssim 2.4$  and  $\gtrsim 4.4$ ), so they will have little bearing on our DLA reddening results because the fewest DLAs are found in quasars at these emission redshifts (see Fig. 1). We therefore conclude that the magnitude and

colour-selection criteria for spectroscopic follow-up of SDSS quasar candidates has had a negligible effect on our reddening estimates for (sub-)DLAs.

## 6 DISCUSSION

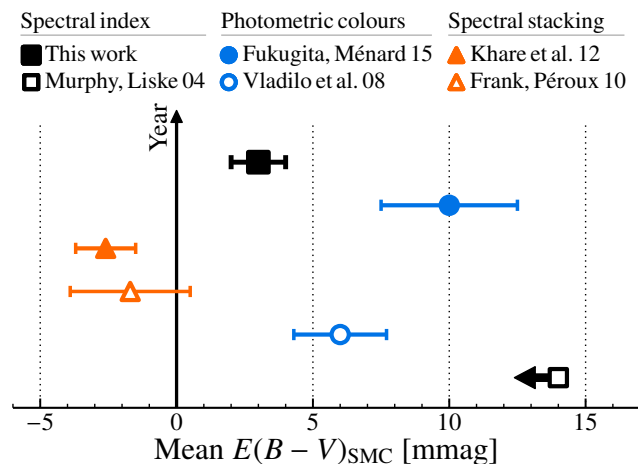
### 6.1 Comparison with recent DLA dust reddening measurements

Figure 12 compares our new DLA dust reddening measurement with those from the other recent studies outlined in Section 1. The six measurements shown are classified according to the methodology used: quasar spectral index measurements, as used in our work here and the early reddening limit from [Murphy & Liske \(2004\)](#); the distribution of quasar photometric colours, as analysed by [Vladilo et al. \(2008\)](#) and, very recently, [Fukugita & Ménard \(2015\)](#); or by analysing composite (‘stacked’) quasar spectra, as in [Frank & Péroux \(2010\)](#) and [Khare et al. \(2012\)](#). For ease of comparison, all results are cast in terms of the mean colour excess from SMC-like dust,  $E(B-V)_{\text{SMC}}$ , over the whole sample studied. Because all results derive from SDSS data, they all cover a similar redshift range,  $2.2 \lesssim z_{\text{abs}} \lesssim 3.5$ , except [Fukugita & Ménard \(2015\)](#) who restrict their DR9 ( $g-i$ ) colour analysis to  $2.1 < z_{\text{abs}} < 2.3$  to avoid contamination of the  $g$ -band photometry from Ly- $\alpha$  absorption. Finally, the measurements in Fig. 12 are based on DLAs only, except that of [Khare et al. \(2012\)](#): in this case we report the  $E(B-V)_{\text{SMC}}$  value from their ‘S1’ comparison of 1084 quasars with a foreground  $\log(N_{\text{H I}}/\text{cm}^{-2}) \geq 20.0$  absorber and the appropriate control sample<sup>4</sup>.

Figure 12 highlights the apparent disagreement between the extant measurements of  $E(B-V)_{\text{SMC}}$ . Our new measurement is consistent with the photometric colour analysis of [Vladilo et al. \(2008\)](#) at  $\approx 1.1\sigma$ , but somewhat inconsistent with the higher  $E(B-V)_{\text{SMC}}$  value of  $\approx 10$  mmag from the colour analysis of [Fukugita & Ménard \(2015\)](#) (i.e. a  $\approx 2.6\sigma$  difference). And while those two previous colour analyses are consistent with each other, they both differ significantly from the non-detection of [Frank & Péroux \(2010\)](#) using spectral stacking (at  $\approx 2.9$  and  $3.5\sigma$ , respectively) and also the negative result from [Khare et al. \(2012\)](#). Our result differs from these two results from spectral stacking as well. Clearly, taking all the existing measurements at face-value, there is no clear indication which, if any, indicate the correct mean dust reddening in SDSS DLAs. It is therefore worth considering some differences between these measurements, though it is beyond the scope of this paper to test in detail whether they are responsible for the confusing picture in Fig. 12 or not.

Firstly, all these recent results, except the photometric analysis by [Fukugita & Ménard \(2015\)](#), rely on SDSS data subject to essentially the same quasar colour selection

<sup>4</sup> For comparison with our results, the appropriate control sample is that which included quasars with no  $\log(N_{\text{H I}}/\text{cm}^{-2}) \geq 20.0$  absorbers but which may include absorbers identified via metal-lines (at redshifts too low for detecting H I) – see table 1 of [Khare et al. \(2012\)](#). The uncertainty in  $E(B-V)_{\text{SMC}}$  used in Fig. 12, 1.1 mmag, is the  $1\sigma$  bootstrap error for their ‘S3’ sample of 545 DLAs scaled by  $\sqrt{545/1084}$ .



**Figure 12.** Summary of recent SDSS DLA dust reddening measurements, separated by methodology: analysis of spectral indices (Murphy & Liske 2004, and the present paper), photometric colours (Vladilo et al. 2008; Fukugita & Ménard 2015) and stacked spectra (Frank & Péroux 2010; Khare et al. 2012). The dust reddening is characterised by the mean colour excess for SMC-like dust,  $E(B-V)_{\text{SMC}}$ , and  $1-\sigma$  error bars are given for all points (see text).

algorithm. It is therefore unlikely that the discrepancies between the results in Fig. 12 are principally explained by such selection effects, especially given our demonstration in Section 5 of their very weak influence. The DR9 quasar selection function differs substantially from earlier releases, so it remains to be explored whether this might explain the higher  $E(B-V)_{\text{SMC}}$  value reported by Fukugita & Ménard (2015).

Secondly, Frank & Péroux (2010) pointed out some difficulties in accurately measuring  $E(B-V)_{\text{SMC}}$  from the ratio of stacked DLA and non-DLA quasar spectra. They discuss how the emission line structure of the quasar spectra bluewards of  $\sim 1700$  Å in the DLA rest-frame, especially the well-known complexes of Fe lines, may limit the accuracy of their ratio spectra in this region. Indeed, they observe a distinct “kink” around  $\sim 1700$  Å in their ratio spectra, noting that it was the main driver towards low  $E(B-V)_{\text{SMC}}$  values. Visual inspection of their figures 4 & 5 suggests a tendency for the DLA–non-DLA ratio stack to be bluer at wavelengths  $\lesssim 1800$  Å and redder between  $\sim 1800$ – $2500$  Å. Frank & Péroux (2010) noted the composite spectrum redwards of  $1700$  Å resulted in a more positive but still null  $E(B-V)_{\text{SMC}}$ . It is therefore possible that analysis of a restricted wavelength range in stacking analyses may be consistent with our result.

In our analysis, the control quasars for a given DLA quasar must satisfy equations (2) and (3), i.e. they must lie at similar emission redshifts and their DLA search paths must span the redshift of the DLA in question, respectively. The latter criterion effectively imposes the same SNR requirements in the Ly- $\alpha$  forest of the control quasar spectra that allowed the detection of the DLA in the DLA quasar’s spectrum. That is, equations (2) and (3), together with the SDSS quasar magnitude and colour selection criteria, ensure that the control quasars are selected with the same restrictions that define the DLA quasar: the same DLA could have been identified in all the control quasars at the same

redshift. Vladilo et al. (2008), Frank & Péroux (2010) and Khare et al. (2012) did not impose equation (3), and instead imposed a magnitude restriction: the control quasars needed to match the corresponding DLA quasar’s  $i$  or  $z$ -band magnitudes ( $\delta z = 0.5$  mag,  $\delta i = 0.08$  and  $0.4$  mag, respectively). However, not imposing equation (3) in our analysis would have artificially biased our results towards zero or even negative reddening, as can be seen via the following example. First, assume that DLAs cause no reddening and that we did not impose equation (3) on control quasars. The control quasars would therefore be allowed to have lower SNR at bluer wavelengths – i.e. over the DLA search path in the Ly- $\alpha$  forest – than any corresponding DLA quasar could have. This (together with the SDSS  $i$ -band magnitude selection criteria) implies that the control quasars would have a redder distribution of colours than the DLA quasars at any given redshift. Restricting instead the  $i$ -band magnitude difference between DLA quasars and their control quasars would not avoid this bias. This is because control quasars would still be allowed to have lower SNR at bluer wavelengths (over the DLA search path) and, therefore, to have redder spectra, than any corresponding DLA quasar could have, even if they all have the same  $i$ -band magnitude. Thus, removing equation (3) would tend to cancel any small reddening signal from the DLAs in our analysis, or even result in a negative mean  $E(B-V)$ , and imposing  $i$ -band magnitude matching would not alter this bias substantially.

Finally, we note that Vladilo et al. (2008) removed all identified sub-DLAs and low-redshift metal-line absorbers from both their DLA and non-DLA samples. Our approach, and that of most previous studies, is to leave such contaminants in both samples, thereby avoiding the significant task of identifying such absorbers. In principle, the approaches are equivalent: these other absorbers are assumed to be unrelated to the DLAs of interest, so should affect the DLA and non-DLA/control samples in the same way and leave a negligible residual in the differential measurement of  $E(B-V)$ .

As discussed in Section 4.4, one aspect of our new result that lends additional confidence that the  $E(B-V)$  detection is really due to DLA dust, is the observed correlation between  $E(B-V)$  and metal-line strength (or metallicity) in Figs. 7, 8 and 9. Vladilo et al. (2008) and Khare et al. (2012) also found a marginal increase in reddening for DLAs with  $W_r(\text{Si II } \lambda 1526) > 1$  Å ( $\approx 1.5\text{-}\sigma$  and  $\approx 2.1\text{-}\sigma$ , respectively), whereas Frank & Péroux (2010) found no dependence on metal content. In our results,  $E(B-V)$  tends to zero as the equivalent width of metal absorption approaches zero, which further suggests that the  $E(B-V)$  values are accurate. A systematic effect that could mimic this tendency is not immediately obvious. Nevertheless, the lowest equivalent-width bins appear slightly ( $<2\text{-}\sigma$ ) below zero reddening, suggesting the possibility that our  $E(B-V)$  measurements could be slightly underestimated. The results of linear fits of  $E(B-V)$  vs.  $W_r(\text{Si II } \lambda 1526)$  and  $W_r(\text{C II } \lambda 1334)$  in Table 5 provide weak evidence ( $<2\text{-}\sigma$ ) that the underestimate in  $E(B-V)_{\text{SMC}}$  could even be  $\approx 4$  mmag (cf. the overall average of 3 mmag). A correction of this size would bring our result into greater consistency with the photometric colour analyses of Vladilo et al. (2008) and Fukugita & Ménard (2015). However, given the low (*post facto*) statistical significance of this possibility, we do not make this correction here; testing it with greater confidence awaits a significantly larger sample of DLA quasars.

## 6.2 The very low average dust content of SDSS DLAs

It is clear from Fig. 12 that most DLAs towards SDSS quasars contain very little dust. This was already apparent from the limit imposed by the first SDSS study, [Murphy & Liske \(2004\)](#), which was inconsistent with earlier results from small DLA and control quasar samples, and it has clearly been confirmed by subsequent studies. However, as noted above, Fig. 12 shows considerable variance in the conclusions reached by different studies about the mean DLA dust reddening. There is not even a clustering of values to provide a guide, only a hint that a reasonable mean value is  $E(B-V)_{\text{SMC}} \sim 2\text{--}10$  mmag. Unfortunately, this observational status precludes a detailed comparison of the mean dust content with other probes of dust in DLAs, or with models for the effect on estimates of  $\Omega_{\text{g}}^{\text{DLA}}$ . Nevertheless, some simple comparisons are illustrative.

One other clear signature of dust in DLAs is the relative depletion of volatile and refractory elements (e.g. Zn vs. Fe, respectively) from the gas phase onto dust grains. Such depletion indicators can be determined in DLAs towards quasars bright enough to provide echelle or echellette spectra with high SNR. For a “typical” DLA at  $z_{\text{abs}} \sim 3$ , the metallicity may be  $[\text{Zn}/\text{H}] \approx -1.5$  (e.g. [Rafelski et al. 2012](#); [Jorgenson et al. 2013](#)) and the dust depletion characterised by  $[\text{Zn}/\text{Fe}] \approx 0.3$  (e.g. [Wolfe et al. 2005](#)), implying  $E(B-V)_{\text{SMC}} \approx 5$  mmag for a DLA with  $N_{\text{H I}} = 10^{21} \text{ cm}^{-2}$  ([Murphy & Liske 2004](#)). Clearly, given the large ranges in DLA metallicity, column density and  $[\text{Zn}/\text{Fe}]$  observed,  $E(B-V)$  is also expected to vary considerably, though a mean  $E(B-V)_{\text{SMC}} > 1$  mmag appears likely. That is, a mean dust reddening of  $E(B-V)_{\text{SMC}} \sim 2\text{--}10$  mmag is consistent with the dust depletion signatures seen in DLAs towards brighter quasars. Naively, we might have expected the latter to have systematically low dust content because of the quasar brightness selection. However, it appears that this must be a small effect. It is also plausible that it may be overwhelmed by other effects, such as gravitational lensing, which might bias such ‘echelle DLAs’ to preferentially probe dustier environments closer to galaxies than the mean SDSS DLA. A similar effect may potentially explain why molecular hydrogen is detected somewhat more often in ‘echelle DLAs’ than in SDSS DLAs ([Jorgenson et al. 2014](#)).

The extent to which dust in DLAs removes quasars, and therefore high- $N_{\text{H I}}$  DLAs, from optically-selected quasar samples, and the possible consequences for  $\Omega_{\text{g}}^{\text{DLA}}$ , has remained an important concern since it was raised by [Ostriker & Heisler \(1984\)](#) and the measurements of [Pei et al. \(1991\)](#) implied it was indeed an important effect. However, this concern has been substantially diminished by SDSS DLA reddening studies and comparisons of DLA distributions in radio and optically selected quasar samples (e.g. [Ellison et al. 2001](#); [Akerman et al. 2005](#); [Jorgenson et al. 2006](#)). Using a Bayesian analysis of a simple dust extinction model, [Pontzen & Pettini \(2009\)](#) considered the joint constraints offered by these radio-optical comparisons and the photometric reddening results of [Vladilo et al. \(2008\)](#) to limit the likely fraction of DLAs missing from optical samples to just 7 per cent ( $1\text{-}\sigma$  confidence). Replacing [Vladilo et al. \(2008\)](#)’s estimate of the mean SDSS DLA reddening with our new measurement, which is a factor of 2 smaller, would reduce this

expected missing fraction below 5 per cent at  $1\text{-}\sigma$  confidence. And while it is always possible to hypothesize that the dust extinction is bimodal in DLAs (e.g. [Khare et al. 2007](#)), the dusty population is clearly small. This seems consistent with the paucity of detections of the 2175 Å ‘dust bump’ and  $10\text{ }\mu\text{m}$  silicate feature in DLAs ([Junkkarinen et al. 2004](#); [Noterdaeme et al. 2009a](#); [Kulkarni et al. 2007, 2011](#)), though the strong selection biases employed to find those systems make a quantitative comparison difficult.

## 7 CONCLUSIONS

Using spectral slope fits of the SDSS DR7 quasar spectra, and the DLA/sub-DLA identifications of [Noterdaeme et al. \(2009b\)](#), we found that the 774 selected quasars with a single foreground DLA are significantly ( $3.2\text{-}\sigma$ ) redder, on average, than carefully selected control groups drawn from a sample of  $\approx 7000$  quasars without foreground DLAs. The detection strengthens to  $4.8\text{-}\sigma$  if sub-DLAs with  $\log(N_{\text{H I}}/\text{cm}^{-2}) \geq 20.0$  are included (a total of 1069 absorber quasars and  $\approx 6700$  control quasars). The reddening corresponds to a mean, rest-frame colour excess due to SMC-like dust of  $E(B-V)_{\text{SMC}} = 3.0 \pm 1.0$  mmag for DLAs at redshifts  $z_{\text{abs}} = 2.1\text{--}4.0$  [ $3.6 \pm 0.9$  mmag when including sub-DLAs]. The DLA colour excess correlates significantly with metal-line (rest-frame) equivalent width, particularly  $W_{\text{r}}(\text{Si II } \lambda 1526)$  ( $\approx 3.5\text{-}\sigma$ ), with  $E(B-V)_{\text{SMC}}$  increasing by  $5.0 \pm 1.4$  mmag per  $1\text{ }\text{\AA}$  increase in  $W_{\text{r}}(\text{Si II } \lambda 1526)$ , for example. This provides further confidence in the reddening detection and that it is really caused by dust in the DLAs. Weaker, less significant correlations are seen with C II equivalent width and the metallicity derived from its known correlation with  $W_{\text{r}}(\text{Si II } \lambda 1526)$ .

No evolution of  $E(B-V)$  in DLAs with redshift was detected, with a  $1\text{-}\sigma$  limit of  $\approx 2.5$  mmag per unit redshift for SMC-like dust. However, this is consistent with the weak DLA metallicity evolution observed in the same redshift range ([Rafelski et al. 2012](#); [Jorgenson et al. 2013](#)) which, assuming a simple proportionality with dust column, implies an increase in  $E(B-V)_{\text{SMC}}$  of only  $\approx 1.3$  mmag per unit (decreasing) redshift. Similarly, no significant dependence of  $E(B-V)$  on the neutral hydrogen column density of DLAs is observed. Nevertheless, the data are consistent with a linear relationship and the implied  $E(B-V)/N_{\text{H I}}$  ratio [e.g.  $(3.5 \pm 1.0) \times 10^{-24} \text{ mag cm}^2$  for SMC-like dust] is consistent with the ratios found in the Magellanic clouds after accounting for the significantly lower typical metallicity of DLAs. However, given the large spread in DLA metallicities, the expected slope of any underlying dust–gas relationship in DLAs may not be reliably comparable with that of the Magellanic clouds.

The very low dust-content of DLAs we find is consistent with that implied by relative metal abundances derived from high-resolution (echelle) spectra of typically much brighter, inhomogeneously selected quasars. It is also consistent with the previously-reported ( $\approx 3\text{-}\sigma$ ) detection by [Vladilo et al. \(2008\)](#) using SDSS DR5 quasar photometric colours, but significantly smaller than that implied by DR9 photometry ([Fukugita & Ménard 2015](#)) and inconsistent with the null results from stacking DR7 quasar spectra ([Frank & Péroux 2010](#); [Khare et al. 2012](#)). Clarifying this somewhat confusing observational picture of the mean DLA dust-content will re-



quire further, independent measurements. Nevertheless, assuming simple relations between dust extinction,  $N_{\text{H}}$ , and metallicity, and including constraints from radio-selected DLA surveys, it remains clear that DLAs dusty enough to be missing from optically-selected samples are rare ( $\lesssim 5$  per cent, cf. Pontzen & Pettini 2009).

Finally, we demonstrated that the magnitude and colour selection of SDSS quasars leads to  $<5\%$  bias in the reddening over the redshift range of interest,  $z = 2.1\text{--}4.0$ . Therefore, the above results do not include corrections for, or systematic error components from, this potential effect. Our code for emulating the SDSS colour-selection algorithm of Richards et al. (2002) is publicly available in Bernet & Murphy (2015). Significantly improving the precision with which dust-reddening can be measured in DLAs will rely on substantially increasing the sample of quasar spectra with accurate photometry and/or spectrophotometry. Although much larger catalogues of quasars are now available from SDSS (e.g. DR10, Pâris et al. 2014), a more accurate measurement of DLA reddening against the ( $\approx 25$ -times larger) natural spread in quasar colours may demand detailed accounting for the quasar selection criteria.

## ACKNOWLEDGEMENTS

We thank J. Xavier Prochaska and Jochen Liske for many helpful discussions and Pasquier Noterdaeme for providing the redshift paths search for DLAs in his DR7 catalogue. We acknowledge the anonymous referee for helpful comments that clarified important aspects of the manuscript. We thank the Australian Research Council for a *QEII Research Fellowship* (DP0877998) and for *Discovery Project* grant DP130100568 which supported this work.

Funding for the SDSS and SDSS-II has been provided by the Alfred P. Sloan Foundation, the Participating Institutions, the National Science Foundation, the U.S. Department of Energy, the National Aeronautics and Space Administration, the Japanese Monbukagakusho, the Max Planck Society, and the Higher Education Funding Council for England. The SDSS Web Site is <http://www.sdss.org/>. The SDSS is managed by the Astrophysical Research Consortium for the Participating Institutions<sup>5</sup>.

<sup>5</sup> The Participating Institutions are the American Museum of Natural History, Astrophysical Institute Potsdam, University of Basel, University of Cambridge, Case Western Reserve University, University of Chicago, Drexel University, Fermilab, the Institute for Advanced Study, the Japan Participation Group, Johns Hopkins University, the Joint Institute for Nuclear Astrophysics, the Kavli Institute for Particle Astrophysics and Cosmology, the Korean Scientist Group, the Chinese Academy of Sciences (LAMOST), Los Alamos National Laboratory, the Max-Planck-Institute for Astronomy (MPIA), the Max-Planck-Institute for Astrophysics (MPA), New Mexico State University, Ohio State University, University of Pittsburgh, University of Portsmouth, Princeton University, the United States Naval Observatory, and the University of Washington.

## REFERENCES

- Akerman C. J., Ellison S. L., Pettini M., Steidel C. C., 2005, *A&A*, **440**, 499
- Aller M. C., Kulkarni V. P., York D. G., Vladilo G., Welty D. E., Som D., 2012, *ApJ*, **748**, 19
- Aller M. C., Kulkarni V. P., York D. G., Welty D. E., Vladilo G., Liger N., 2014, *ApJ*, **785**, 36
- Asplund M., Grevesse N., Sauval A. J., Scott P., 2009, *ARA&A*, **47**, 481
- Becker R. H., White R. L., Helfand D. J., 1995, *ApJ*, **450**, 559
- Bernet M. L., Murphy M. T., 2015, SDSS\_QSOsel\_Bernet: First release, [doi:10.5281/zenodo.31470](https://doi.org/10.5281/zenodo.31470)
- Cardelli J. A., Clayton G. C., Mathis J. S., 1989, *ApJ*, **345**, 245
- Crichton N. H. M. et al., 2015, *MNRAS*, **452**, 217
- Draine B. T., 2003, *ARA&A*, **41**, 241
- Ellison S. L., Yan L., Hook I. M., Pettini M., Wall J. V., Shaver P., 2001, *A&A*, **379**, 393
- Ellison S. L., Hall P. B., Lira P., 2005, *AJ*, **130**, 1345
- Fall S. M., Pei Y. C., 1989, *ApJ*, **337**, 7
- Fall S. M., Pei Y. C., 1993, *ApJ*, **402**, 479
- Fall S. M., Pei Y. C., McMahon R. G., 1989, *ApJ*, **341**, L5
- Fitzpatrick E. L., 1985, *ApJ*, **299**, 219
- Frank S., Péroux C., 2010, *MNRAS*, **406**, 2235
- Fukugita M., Ménard B., 2015, *ApJ*, **799**, 195
- Jenkins E. B., 1987, in Hollenbach D. J., Thronson Jr. H. A., eds, *Astrophys. Space Sci. Libr. Vol. 134, Interstellar Processes*. pp 533–559
- Jenkins E. B., Peimbert A., 1997, *ApJ*, **477**, 265
- Jiang P., Ge J., Prochaska J. X., Wang J., Zhou H., Wang T., 2010, *ApJ*, **724**, 1325
- Jorgenson R. A., Wolfe A. M., Prochaska J. X., Lu L., Howk J. C., Cooke J., Gawiser E., Gelino D. M., 2006, *ApJ*, **646**, 730
- Jorgenson R. A., Murphy M. T., Thompson R., 2013, *MNRAS*, **435**, 482
- Jorgenson R. A., Murphy M. T., Thompson R., Carswell R. F., 2014, *MNRAS*, **443**, 2783
- Junkkarinen V. T., Cohen R. D., Beaver E. A., Burbidge E. M., Lyons R. W., Madejski G., 2004, *ApJ*, **614**, 658
- Kaplan K. F., Prochaska J. X., Herbert-Fort S., Ellison S. L., Dessauges-Zavadsky M., 2010, *PASP*, **122**, 619
- Khare P., Kulkarni V. P., Péroux C., York D. G., Lauroesch J. T., Meiring J. D., 2007, *A&A*, **464**, 487
- Khare P., Vanden Berk D., York D. G., Lundgren B., Kulkarni V. P., 2012, *MNRAS*, **419**, 1028
- Kulkarni V. P., York D. G., Vladilo G., Welty D. E., 2007, *ApJ*, **663**, L81
- Kulkarni V. P., Torres-Garcia L. M., Som D., York D. G., Welty D. E., Vladilo G., 2011, *ApJ*, **726**, 14
- Kurt C. M., Dufour R. J., 1998, in Dufour R. J., Torres-Peimbert S., eds, *Revista Mexicana de Astron. Astrofísica Conf. Series Vol. 7, The sixth Texas-Mexico conference on astrophysics: astrophysical plasmas – near and far*. p. 202
- Lanzetta K. M., Wolfe A. M., Turnshek D. A., 1995, *ApJ*, **440**, 435
- Ledoux C., Bergeron J., Petitjean P., 2002, *A&A*, **385**, 802
- Ledoux C., Petitjean P., Srianand R., 2003, *MNRAS*, **346**, 209
- Ma J. et al., 2015, *MNRAS*, **454**, 1751
- Martin N., Maurice E., Lequeux J., 1989, *A&A*, **215**, 219
- Murphy M. T., Liske J., 2004, *MNRAS*, **354**, L31
- Neeleman M., Wolfe A. M., Prochaska J. X., Rafelski M., 2013, *ApJ*, **769**, 54
- Newberg H. J., Yanny B., 1997, *ApJS*, **113**, 89
- Noterdaeme P., Ledoux C., Srianand R., Petitjean P., Lopez S., 2009a, *A&A*, **503**, 765
- Noterdaeme P., Petitjean P., Ledoux C., Srianand R., 2009b, *A&A*, **505**, 1087
- O'Donnell J. E., 1994, *ApJ*, **422**, 158



- Ostriker J. P., Heisler J., 1984, *ApJ*, **278**, 1
- Pâris I. et al., 2012, *A&A*, **548**, 66
- Pâris I. et al., 2014, *A&A*, **563**, A54
- Pei Y. C., 1992, *ApJ*, **395**, 130
- Pei Y. C., Fall S. M., Bechtold J., 1991, *ApJ*, **378**, 6
- Pettini M., King D. L., Smith L. J., Hunstead R. W., 1997, *ApJ*, **478**, 536
- Pontzen A., Pettini M., 2009, *MNRAS*, **393**, 557
- Prochaska J. X., Wolfe A. M., 2009, *ApJ*, **696**, 1543
- Prochaska J. X., Herbert-Fort S., Wolfe A. M., 2005, *ApJ*, **635**, 123
- Prochaska J. X., Chen H.-W., Wolfe A. M., Dessauges-Zavadsky M., Bloom J. S., 2008, *ApJ*, **672**, 59
- Rafelski M., Wolfe A. M., Prochaska J. X., Neeleman M., Mendez A. J., 2012, *ApJ*, **755**, 89
- Reichard T. A. et al., 2003, *AJ*, **125**, 1711
- Richards G. T. et al., 2002, *AJ*, **123**, 2945
- Schlegel D. J., Finkbeiner D. P., Davis M., 1998, *ApJ*, **500**, 525
- Schneider D. P. et al., 2007, *AJ*, **134**, 102
- Schneider D. P. et al., 2010, *AJ*, **139**, 2360
- Shen Y. et al., 2011, *ApJS*, **194**, 45
- Vanden Berk D. E. et al., 2001, *AJ*, **122**, 549
- Viegas S. M., 1995, *MNRAS*, **276**, 268
- Vladilo G., 2002, *ApJ*, **569**, 295
- Vladilo G., Péroux C., 2005, *A&A*, **444**, 461
- Vladilo G., Prochaska J. X., Wolfe A. M., 2008, *A&A*, **478**, 701
- Wang J., Hall P. B., Ge J., Li A., Schneider D. P., 2004, *ApJ*, **609**, 589
- Wang J.-G. et al., 2012, *ApJ*, **760**, 42
- Wolfe A. M., 1986, *R. Soc. London Philos. Trans. Series A*, **320**, 503
- Wolfe A. M., Turnshek D. A., Smith H. E., Cohen R. D., 1986, *ApJS*, **61**, 249
- Wolfe A. M., Prochaska J. X., Gawiser E., 2003a, *ApJ*, **593**, 215
- Wolfe A. M., Gawiser E., Prochaska J. X., 2003b, *ApJ*, **593**, 235
- Wolfe A. M., Gawiser E., Prochaska J. X., 2005, *ARA&A*, **43**, 861
- Zhou H., Ge J., Lu H., Wang T., Yuan W., Jiang P., Shan H., 2010, *ApJ*, **708**, 742

## APPENDIX A: EMULATING THE SDSS QUASAR SELECTION ALGORITHM

In this Appendix we briefly review the approach followed by Richards et al. (2002) to select quasar candidates, based on their SDSS photometric magnitudes and colours, for spectroscopic follow-up. We demonstrate that our emulation of this approach performs appropriately for the purposes of this paper, primarily via the results in Fig. 11 and Figs. A1 & A2.

SDSS quasar candidates were selected via their colours in *ugriz* broadband photometry, specifically the target point-spread-function (PSF) magnitudes in these filters. Broadly speaking, objects were selected as quasar candidates if they were consistent with being point sources and if they fell outside the four dimensional colour space inhabited by the stellar locus (Richards et al. 2002). The colours of ordinary stars occupy a continuous, narrow region in the ‘colour space’ ( $u-g$ )-( $g-r$ )-( $r-i$ )-( $i-z$ ) (Newberg & Yanny 1997) and the stellar temperature is the main parameter that determines the position along this stellar locus. And while stars have approximately blackbody spectra, quasars spectra can be characterized by a power-law overlaid with broad emission lines. Therefore, quasars generally have colours quite distinct from stellar colours and can be identified as outliers from the

stellar locus. The exception to this is the well-known redshift range,  $2.5 \lesssim z_{\text{em}} \lesssim 3.0$  where quasar colours cross the stellar locus.

Newberg & Yanny (1997) modelled the stellar locus as a two-dimensional ribbon with a varying elliptical cross section; more specifically, their locus consisted of a series of overlapping right elliptical cylinders capped with half-ellipsoids. To simplify the algorithm for quasar colour-selection, Richards et al. split the four-dimensional colour space into two three-dimensional colour spaces, *ugri* and *griz*. In essence, an object is then considered a quasar candidate if its colours lie outside the ellipse given by the convolution of the closest stellar colour ellipse and the ellipse formed from the object’s photometric colour errors.

The SDSS quasar selection algorithm consists of checking an object’s target PSF magnitudes and uncertainties against four main criteria:

1. Whether they lie in an ‘exclusion box’, i.e. regions of the colour space in which the too-numerous Galactic contaminants lie, such as white dwarfs, white dwarf pairs, A stars and M stars.
2. Whether they lie more than  $4\text{-}\sigma$  outside the *ugri* stellar locus and  $i \leq 19.1$  (corresponding mainly to quasars at  $z_{\text{em}} < 3.0$ ).
3. Whether they lie more than  $4\text{-}\sigma$  outside the *griz* stellar locus and  $i \leq 20.2$  (corresponding mainly to quasars at  $z_{\text{em}} > 3.0$ ).
4. Whether they lie in an ‘inclusion region’ of colour space (see the specific definitions in section 3.5.2 of Richards et al. 2002). These apply to objects whose colours are consistent with being quasars at:
  - 4.i  $2.5 < z_{\text{em}} < 3.0$ , 10 per cent are selected (based on their right ascension) from those near, but still more than  $2\text{-}\sigma$  outside, the stellar locus (i.e. closer than the usual  $4\text{-}\sigma$  exclusion criterion);
  - 4.ii  $z_{\text{em}} \leq 2.2$ , a simple  $u - g$  colour selection is applied;
  - 4.iii  $z_{\text{em}} > 3.6$ , which are not well selected by the *griz* outlier criteria, further *griz* selection criteria are defined;
  - 4.iv  $z_{\text{em}} > 4.5$ , a selection using *riz* colours is defined.

If an object satisfied criteria 1 and 2, or 1 and 4.i, or 1 and 4.ii, Richards et al. classified it as a “low- $z$  quasar”. If it object satisfied criteria 1 and 3, or 1 and 4.iii, or 1 and 4.iv, it was classified as a “high- $z$  quasar”. One object may be classified as both a low- $z$  and high- $z$  quasar in this way.

We implemented the stellar locus definition and these criteria into a MATLAB code to emulate the SDSS quasar selection algorithm of Richards et al., which we provide in Bernet & Murphy (2015). Potential users of this code should note that several channels for selecting quasar candidates in Richards et al. were not implemented in our code. For example, candidates that are radio sources in the FIRST survey (Becker et al. 1995) were generally included by Richards et al. (see their figure 1). This makes their selection independent of colour, but for this reason it was not important to implement this in our code to test the colour-selection sensitivity of our reddening analysis. Richards et al.’s algorithm also deals with objects that were not detected in some filters. However, this is only important for very faint quasar candidates, or those at  $z_{\text{em}} \gtrsim 4.7$  (where the  $g$ -band flux may be entirely consumed by a Lyman-limit system). These cases are not relevant for our sample selection, so we

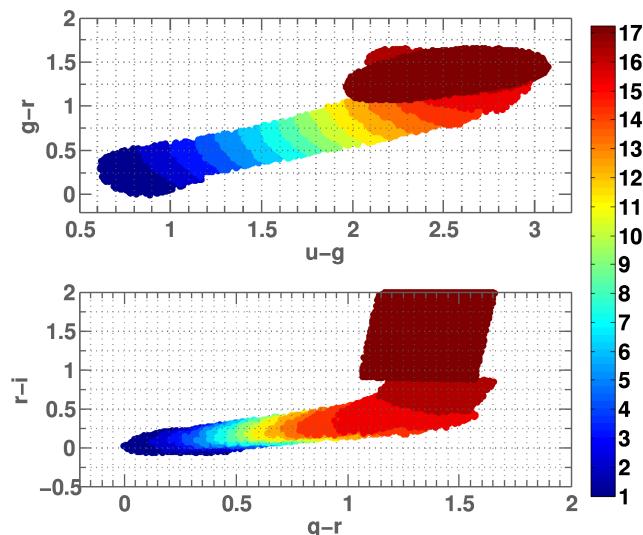


**Figure A1.** The  $g-r$  versus  $u-g$  and  $r-i$  versus  $g-r$  colour-colour planes of the stellar locus in our emulation of the “low- $z$ ” (i.e. *ugri*) SDSS quasar selection criteria Richards et al. (2002). This figure is very similar to their figures 2 & 3. The colour of a plotted point encodes the number of the nearest “stellar locus point”, as defined in table 3 of Richards et al. (2002). The plotted points define the projection of the  $4\text{-}\sigma$  error surface and were determined by Monte Carlo sampling. Objects with zero photometric errors will be selected as quasar candidates if they fall outside this surface. We note that, although our stellar loci plots are very similar to those of Richards et al. (2002), there are some small differences that we can not account for, so users of our code should test it specifically for their purposes to ensure reliable statistical results.

neglect this complication in our code. We also do not implement the criteria used to distinguish point sources from extended objects. Finally, note that the Schneider et al. (2010) DR7 quasar catalogue also contains quasars which were selected as part of a galaxy and luminous red galaxy survey, as showing X-ray emission, in different stellar surveys and via serendipitous detection, as specified in their table 1.

Figures A1 and A2 show the relevant colour-colour planes of the  $4\text{-}\sigma$  error surfaces for the *ugri* and *griz* stellar loci in our code. Objects with zero photometric errors will be selected outside this surface. In practice, points plotted in these diagrams were determined by a simple Monte Carlo test: artificial objects covering the *ugriz* space, all with  $\sigma_{u,g,r,i,z} = 0.0$ , were tested against criteria 2 and 3 above and those objects not selected as quasar candidates were plotted. Figures A1 and A2 are very similar to figures 2 & 3, and 5 & 6 in Richards et al. and demonstrate that the stellar locus is adequately modelled in our code. Nevertheless, some small differences are visually apparent (despite several checks to ensure our code matches the written specifications) and, although these should not have any important effects on our dust-reddening analysis here, we caution that other researchers should test our code for their specific purposes to ensure the reliability of any conclusions they draw.

A further, simple test of our code is to check whether it selects quasar candidates via the same selection channel as specified by Schneider et al. (2010). For this test we use the entire sample of  $2.2 < z_{\text{em}} < 4.42$  quasars in the Noterdaeme

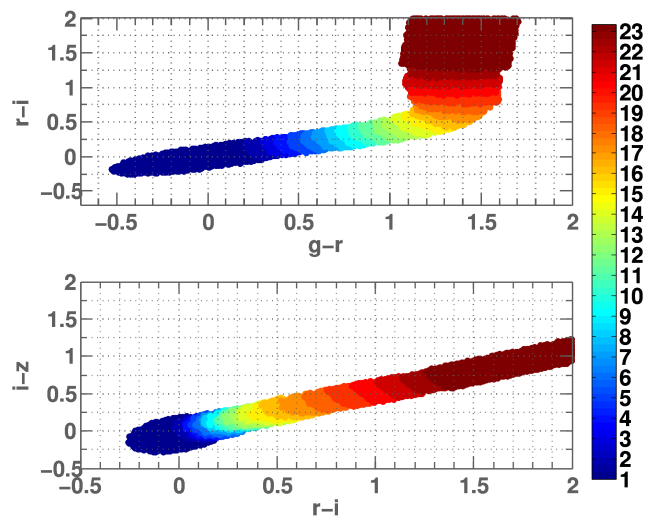


**Figure A2.** Same as Fig. A2 but for the  $r-i$  versus  $g-r$  and  $i-z$  versus  $r-i$  colour-colour plane for the “high- $z$ ” (i.e. *griz*) quasar selection criteria. This figure is very similar to figures 5 & 6 of Richards et al. (2002) and the colour of a plotted point encodes the number of the nearest “stellar locus point” defined their table 4.

et al. (2009b) catalogue from which our reddening analysis stems. Inputting the target PSF photometry of these quasars into our code results in 60 per cent of them being selected via the *ugri* channel and 62 per cent via the *griz* channel (noting that each object can be selected by either, both or neither channel). These values are similar to, though slightly higher than, the values of 51 and 59 per cent, as defined by the classification of Schneider et al. (2010) using the same selection algorithm as in Richards et al. (2002). Again, although these differences are not important for assessing the degree of bias entering our dust-reddening analysis (especially in light of the results in Fig. 10), it is possible that such differences are important for other high-precision, statistical studies with large samples, so we again recommend further, specific reliability tests in those circumstances.

## SUPPORTING INFORMATION

Additional Supporting Information may be found in the online version of this article:

**Table 1.** The DLA quasar sample (774 quasars).

**Table 2.** The absorber quasar sample (1069 quasars).

**Table 3.** The non-DLA quasar sample (7105 quasars).

**Table 4.** The non-absorber quasar sample (6733 quasars).

Please note: Oxford University Press are not responsible for the content or functionality of any supporting materials supplied by the authors. Any queries (other than missing material) should be directed to the corresponding author for the paper.

This paper has been typeset from a  $\text{\LaTeX}$  file prepared by the author.